

A new comprehensive classification of the Piton de la Fournaise activity spanning the 1985–2010 period. Search and analysis of short-term precursors from a broad-band seismological station

Geneviève Roult ^{a,b,*}, Aline Peltier ^{b,c}, Benoît Taisne ^{a,b}, Thomas Staudacher ^{b,c,d},
Valérie Ferrazzini ^{b,c,d}, Andrea Di Muro ^{b,c,d} and the OVPF team

^a Equipe de Sismologie, Institut de Physique du Globe de Paris- Sorbonne Paris Cité, 1 rue Jussieu, 75238 Paris Cedex 05, France

^b UMR CNRS 7154, Université Paris Diderot, France

^c Equipe Géologie des Systèmes Volcaniques, Institut de Physique du Globe de Paris- Sorbonne Paris Cité, 1 rue Jussieu, 75238 Paris Cedex 05, France

^d Observatoire Volcanologique du Piton de la Fournaise, 14RN3, 97418 La Plaine des Cafres, La Réunion, France

ARTICLE INFO

Article history:

Received 21 February 2012

Accepted 6 June 2012

Available online 21 June 2012

Keywords:

Piton de La Fournaise

Database

Eruption precursors

Failed eruptions

Broad-band seismic stations

Magma migration

Volcano monitoring

ABSTRACT

Piton de la Fournaise volcano (La Réunion Island) is one of the most active basaltic volcanoes, with an average of one eruption every 10 months. This study provides the first exhaustive compilation of all volcanic events (intrusions, eruptions, seismic crises) and related parameters at Piton de la Fournaise in the 1985–2010 period. This compilation has been correlated with the analysis of the records from the very broad-band seismological RER station (Geoscope network), located 8.5 km north of the summit. Our approach allowed us to identify short-term long period seismic precursors for most eruptions and intrusions. After a signal filtering process that consists in removing the instrumental response and the theoretical Earth tides effect, these precursors can be distributed into 4 classes that depend on their waveform and are globally considered as tilt related with magma transfer inside the sub-aerial part of the volcano edifice. The shapes and characteristics of these transient phenomena (time delay, duration or class) exhibit particular features that can be partly related to other simple eruption or intrusion parameters (location, altitude, volume). Statistical analyses of all events (intrusions and eruptions) are then derived. Estimates of acceleration rates of tilt signal at the RER station have been retrieved for eruptions and intrusions, with the challenge of providing a way to differentiate one from the other in real-time. Acceleration rates seem to correlate with eruptive lava flow volume and a threshold value can be determined allowing us to discriminate between intrusions and eruptions, illustrating the interest of analyzing them for real-time monitoring. The correlation with the initial seismic crisis marking the opening of magma ascent path was investigated, showing that the delay between the RER transient phenomenon and the start of the seismic crisis has been increasing since the major caldera formation event of 2007. This longer delay may be due to a combination of drastic changes in the internal structure of the edifice: a concomitant decrease in volume of magma batches and a deeper origin of magma setting off volcanic unrest. Our study highlights the additional role of external factors like loading and unloading related to the rainy season and stress field evolution due to Earth tides in influencing magma propagation and volcanic activity.

© 2012 Elsevier B.V. All rights reserved.

1. Introduction

The predictability of earthquakes or volcanic eruptions, allowing short-term hazard mitigation, remains a challenging problem. Forecast of volcano behavior (intrusion versus eruption) is still an extremely difficult task. We use the term “intrusion” when no

eruption ensues. Both intrusions and eruptions are often preceded by a seismic crisis. Early discrimination between these phenomena, during the seismic crisis, may be attempted either with a multi-parameter approach (ground deformation, seismicity, degassing), or by searching for subtle eruptive precursors (see [Dzurisin, 2003](#) for a complete review; [Brenguier et al., 2008](#) and [Peltier et al., 2009a](#) for the case of Piton de La Fournaise). This research can best be conducted on a well-monitored volcano, displaying frequent eruptive activity. Piton de La Fournaise, with an average of one eruption every 10 months, appears to be a good target for such a study.

* Corresponding author at: Equipe de Sismologie, Institut de Physique du Globe de Paris, Sorbonne Paris Cité, 1 rue Jussieu, 75238 Paris Cedex 05, France.

E-mail address: groult@ipgp.fr (G. Roult).

Piton de La Fournaise volcano (La Réunion hot spot, Fig. 1a, b) is one of the most active basaltic shield volcanoes in the world, with the occurrence of 54 eruptions and at least 11 intrusions since December 1985. Eruptive vents and lava flows found during each of those eruptions are reported in Fig. 1c. Typically, each intrusion or eruption is preceded by weeks/months of inflation of the summit cone and an increasing number of shallow (above sea level) volcano-tectonic events and rock-falls (particularly since the 2007 collapse). Several networks have been maintained by the Volcano Observatory of Piton de la Fournaise (OVPF) since 1979 to monitor the volcano activity: short-period seismic stations, broad-band seismic stations since 2009, tiltmeters, extensometers, GPS stations, DOAS and MultiGas stations. In addition to the seismic stations installed by the OVPF on the volcano, one of the first broad-band stations of the global seismological GEOSCOPE network, was installed close to the Volcano Observatory in 1982, 15.3 km from the crater (Fig. 1a), the PCR seismic station (Plaine des Cafres, la Réunion). This station was equipped with three high-quality Streckeisen seismometers (STS-1, Wielandt and Streckeisen, 1982). In the beginning for the GEOSCOPE network, the only recording channels corresponded to the ground acceleration and the transfer function of the acquisition chain in 12 bits was flat in the 0.01–3600 s period range (Romanowicz et al., 1991). Due to bad environmental conditions, the noise power spectral density was high. At the time the challenge of the GEOSCOPE network, affiliated to FDSN (Federation of Digital Seismographic Networks), became the availability of very-broad band data in real-time. We decided to progressively upgrade all the GEOSCOPE stations and to move the acquisition chain from a broad-band configuration to a very-broad band configuration in 24 bits (Roult et al., 2010). The STS-1 seismometers of the PCR station were moved to a new site in February 1986, at RER (Rivière de l'Est, La Réunion; Fig. 1a), 8.5 km north of the summit crater. This station is located at 21.171 S, 55.741 E, at an elevation of 834 m, in a vault corresponding to a 4.7 km long tunnel that highly reduces the noise due to temperature variations. It has been operational for 25 years (apart from the February 11th 2003 to September 5th 2004 breakdown period). The sensors, installed on a glass plate, are covered with a permalloy shielding (vertical only), an aluminum shielding and a glass bell. A styrofoam box, sheeted with aluminum is put over each sensor as a protection against fast changes in temperature and air flow. A second important upgrade occurred in 1990. The new equipment consisted of the three same STS-1 connected to a Q330HR digitizer; the available seismic channels record either the ground velocity (BH*, LH*, VH*) or the ground acceleration (boom position, LM*). Before 1990, the large number of glitches on the recordings and the low sensitivity of the acquisition chain made the observation of eruption precursory signals very difficult. The high sensitivity of the acquisition chain since 1990, allowed a better identification of transient signals due to the Piton de la Fournaise activity. In September 2010 the sensitivity increased even more with a new upgrade of the station by a 26 bit acquisition chain. Short-term precursors have thus been identified in the form of long period signals that occur mostly on the RER horizontal components during the minutes or hours that accompany magma migration. Battaglia et al. (2000) first reported such transients for 5 eruptive events from July 1991– March 1998 at RER station. Houlié and Montagner (2007) also distinguished two kinds of transients from the 1998–2005 RER records. Up to now no exhaustive and complete study from the RER station analysis exists in the literature.

In this study, we first compiled information on all volcanic events (eruptions, intrusions, seismic crises, pit craters and caldera collapses) at Piton de La Fournaise that have occurred since

December 1985 (i.e. a few months before the RER station installation) and established a comprehensive database. Then, we systematically retrieved and analyzed the RER recordings corresponding to all these events. Statistical analyses of the characteristics of all eruptions and intrusions allow us to discuss the volcanic processes associated to the RER transient precursors. This work, with the presentation of a new comprehensive compilation of eruption/intrusion characteristics since December 1985, also aims to provide a working database for future studies on Piton de La Fournaise.

2. A comprehensive Piton De La Fournaise database

We have extracted as much information as possible on all eruptive events spanning the 1985–2010 period to allow further studies on Piton de la Fournaise behavior and transient modeling. The database is presented on Appendix A. It is subdivided in four distinct sections whose parameters are successively described in Appendixes B, C, D and E, as follows:

- (1) volcanic event characteristics
- (2) parameters of the transient observed at the RER seismological broad-band station
- (3) parameters of the theoretical Earth acceleration tide
- (4) dyke parameters from previous studies.

In this paper we will present these four sub-sections one by one.

In order to fill and complete our catalog of events, we used the monthly OVPF bulletins, the individual recordings, the spectral diurnal analyses for each station belonging to the network, the existing literature and academic works (Bachèlery, 1999; Peltier, 2007), as well as internal OVPF reports (Staudacher, 1992–2008; <http://www.volcano.si.edu/>) and international publications (i.e. Delorme et al., 1989; Lénat et al., 1989; Stieljes and Moutou, 1989; Peltier et al., 2009a). For eruptions spanning the 1985–1987 period we analyzed the “Sefram” paper recordings from 8 seismic stations to gather new information and check previous descriptions.

Our review results in the identification of 83 volcanic events including 54 eruptions, 26 seismic crises not followed by an eruption, 2 summit pit crater formations and 1 caldera collapse. We do not discuss all the listed variables in this paper, but they should serve as an extensive and validated database for further studies. Our large database compilation, covering 25 years of eruptive activity at Piton de La Fournaise, allows us to complete and improve previous observations on the dynamics of the volcano. In the two following sections we will present the eruptive event characteristics and parameters of the associated signals recorded by the distant RER broad-band station.

3. Volcanic event characteristics

The main features of all identified volcanic events are summarized in Appendix A. We considered that two eruptions were distinct (and associated with a specific family type) when each of them was preceded by a distinct seismic crisis. As a consequence of this choice, two ‘apparent’ eruptive events, separated by several hours or days, may be attributed to a single eruption in Appendix A (example March 30th 2007 and April 2nd 2007 eruptive events preceded by a single seismic crisis). The definitions of the volcanic event characteristics under study reported in Appendix A (type, eruption timing, site, fissures, elevation, lava flow, seismic crisis, seismic swarm...) are given in Appendix B.

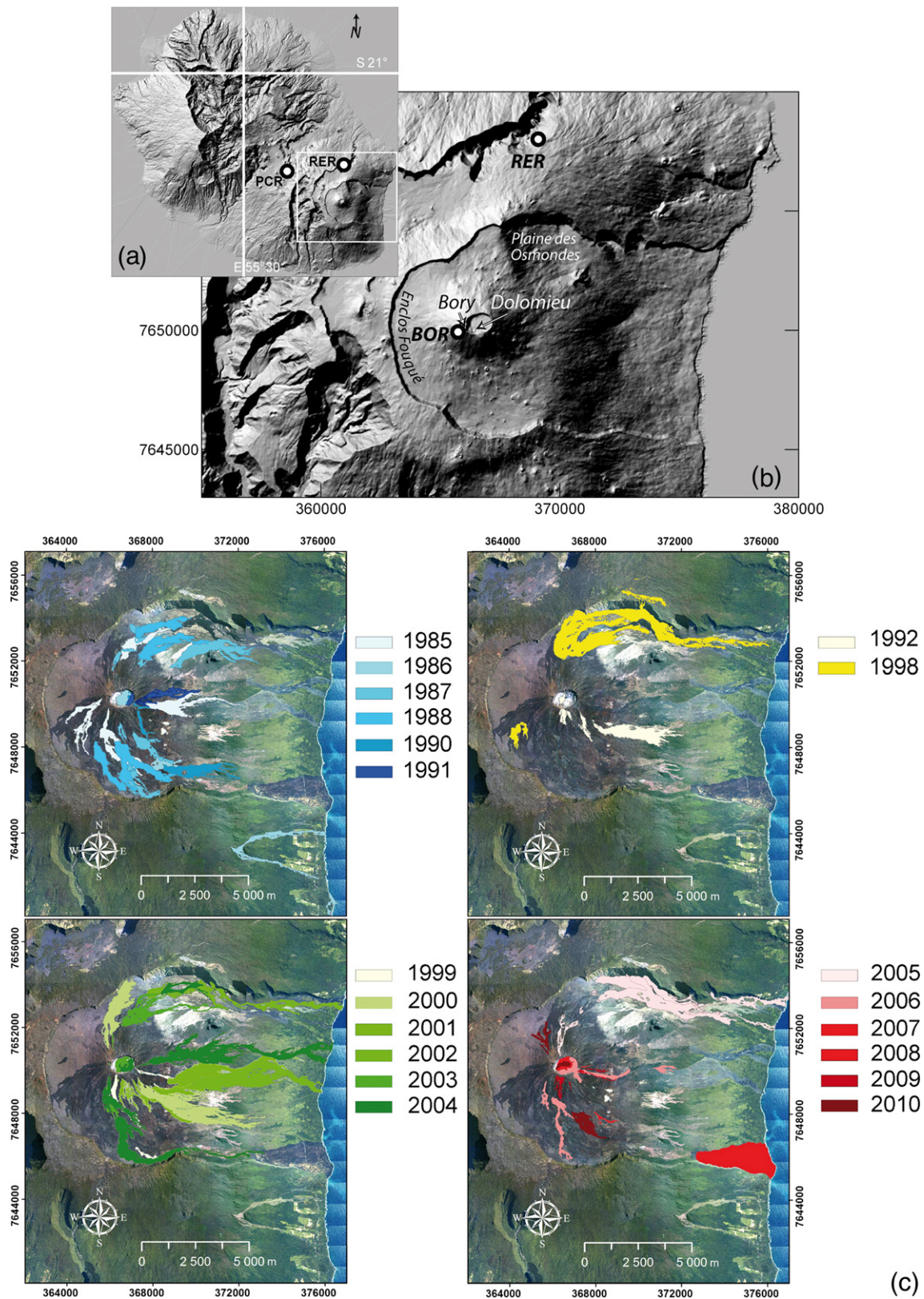


Fig. 1. (a) Location of the Piton de la Fournaise volcano in the Indian Ocean with indication of the PCR (Plaine des Cafres) and RER (Rivière de l'Est) broad-band seismological stations of the GEOSCOPE network, operational from 1982 to 1986 (PCR) and from 1986 to now (RER). (b) Focus on the Piton de La Fournaise volcano with the OVPF BOR (Bory) and the GEOSCOPE RER stations (coordinates in UTM WGS84). (c) Location of the different eruptive episodes in the 1985–2010 period (coordinates in UTM WGS84).

3.1. Eruption family types between 1985 and 2010

At Piton de La Fournaise, the vents of all recent eruptions (post-1515 AD; Tanguy et al., 2011) occur either inside the summit craters or along its eastern flank following one of the rift zones (Bachèlery, 1999). We distinguished three family types of eruptions according to the location of the eruptive fissures: E-C eruptions that begin and remain inside the summit craters, E-CL eruptions that start inside the summit craters and then propagate laterally towards lower elevation and E-L eruptions that start anywhere else, outside of the summit crater (Appendixes A and B). According to deformation analyses of Peltier et al. (2005), all dykes are considered to start below the summit cone and propagate first vertically (during 10 to 50 min; see the corresponding DVI “Duration of Vertical dyke Injection” value in Appendixes A and E), then, some of them propagate laterally and eventually horizontally and give E-CL and E-L eruptions.

The beginning and duration of the eruptive events since December 1985 are plotted in Fig. 2, with an indication of the family type, as described in Appendix B (E for eruption, Co for collapse, SC for seismic crisis, D for deformation, T for tremor). Peltier et al. (2009a) described the volcano behavior as a succession of cycles, inside which eruptions are located at increasing distances from the summit and lower elevations with time, and lava emissions with decreasing K₂O and increasing MgO (olivine) contents (see concentration values of MgO in Appendixes A and E). The “SPD sequence” (each cycle formed by a sequence of summit, proximal and distal eruptions) has been proposed for the 1998–2007 period. These eruptive cycles have been explained by the preferential motion of the eastern flank caused by continuous recharging of the shallow part of the magma system, the eastern flank being the only direction with a free boundary condition (toward the sea). Such motion would favor the occurrence of distal eruptions towards this flank at the end of a cycle. However, our review does not allow us to extrapolate

this model to the whole 1985–2010 period. Moreover, a cyclic behavior is not clearly identified even in the 1998–mid-2003 period.

3.2. Seismicity associated to volcanic events

An eruption at Piton de la Fournaise is usually preceded by an unrest period that may last days or months and is characterized by a slowly increasing seismicity and ground deformation. The onset of a seismic crisis marks the acceleration of the process (Collombet et al., 2003; Peltier et al., 2005, 2009a; Lengliné et al., 2008). It is, in most cases, composed of shallow events located below the central cone, from 0 to 2300 m above sea level. Examples of seismic crises at Piton de La Fournaise are described in Sapin et al. (1996), Massin et al. (2011), Taisne et al. (2011a). Battaglia et al. (2005) describe the exceptional earthquake migration from ~5 km b.s.l. to the surface, observed just prior to the 1998 eruption.

An example of a seismogram recorded at BOR (one of the OVPF short-period seismic stations, located south-west of the Bory crater, see Fig. 1b for location) and its corresponding spectrogram obtained for the October 14th 2010 eruption is given in Fig. 3. Four distinct phases can be identified during the pre-eruptive seismic crises at Piton de La Fournaise. The first one (phase 1) is characterized by an acceleration of the seismicity with a large number of volcano-tectonic (VT) events, more than one event per minute and sometimes overlapping. The second one, the swarm phase (phase 2), is characterized by numerous merged events (more than six events per minute with larger magnitude than in the previous phase). This phase is not always present. The third one (phase 3) corresponds to a seismically quiet/low intensity sequence with a small number of VT events. The fourth and last phase corresponds to the building and stabilization of eruptive tremor, which is, in most cases, associated with the opening of eruptive fissures.

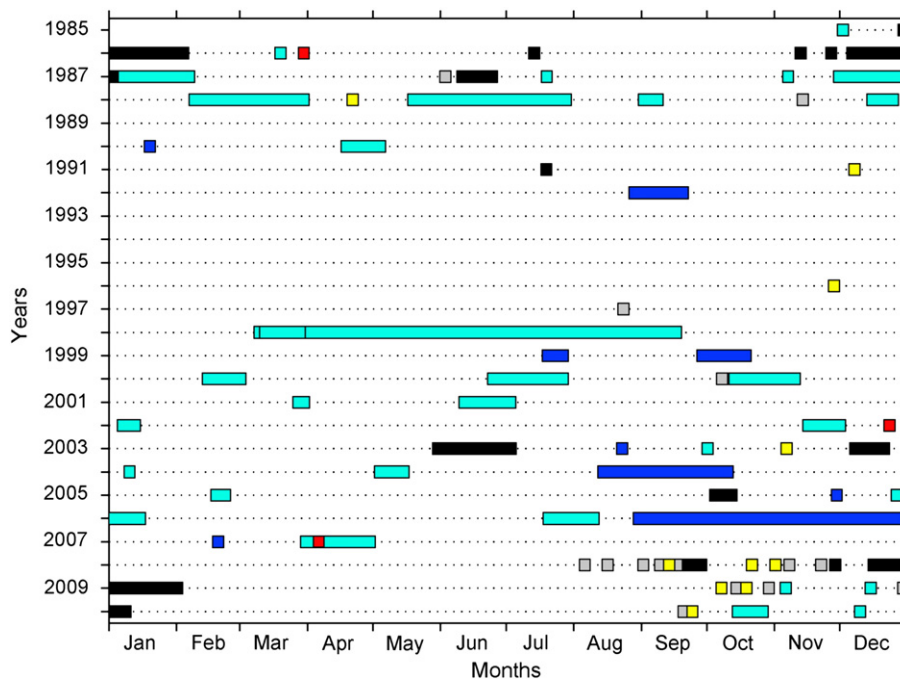


Fig. 2. Distribution and duration of volcanic events in the December 1985–December 2010 period. Onset times and durations, with indication of the family type: eruptions (E-C in black, E-CL in dark-blue, E-L in light-blue), intrusions (SC-D, SC-DT, SC-T in yellow), seismic crises (SC in grey) and collapses (Co in red) for each year. Note the increase in frequency of intrusions and seismic crises after the major 2007 caldera forming eruption.

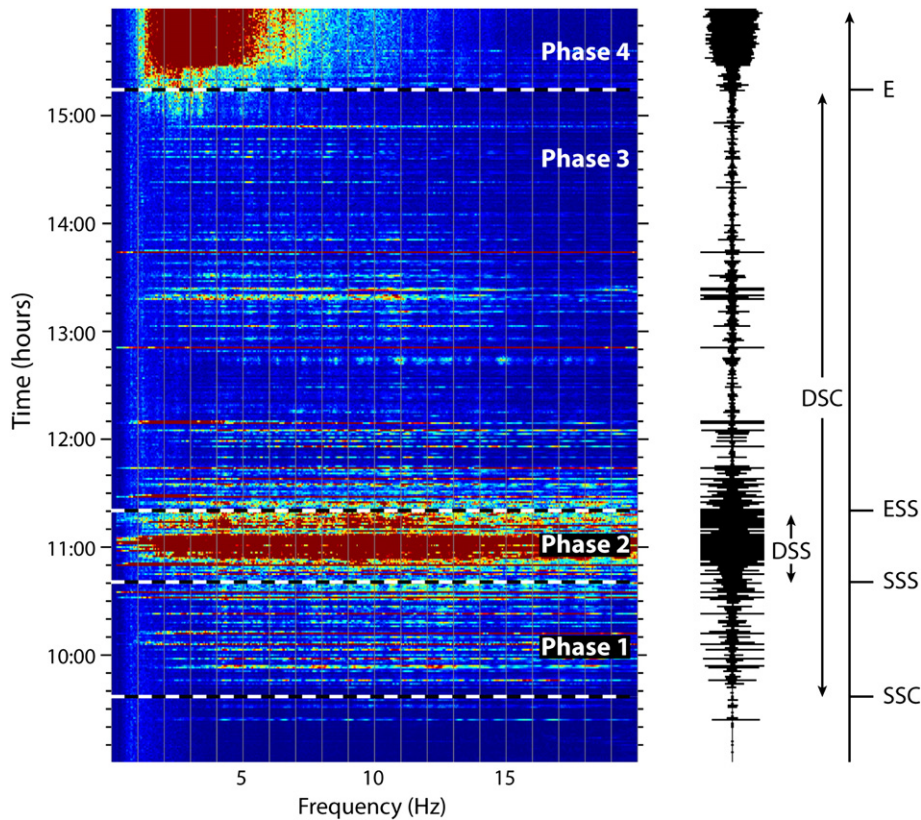


Fig. 3. Definition of some parameters related to typical seismic crises of Pdf volcano as listed in Appendix A. The spectrogram illustrates the main phases identified in the analysis of the power spectral analysis of the short-period seismometer installed at the Bory station (OVPF network). The example corresponds to the October 14th 2010 eruption. SSC is the starting of the seismic crisis, SSS the starting of the seismic swarm, ESS the ending of the seismic swarm, E the onset time of the eruptive tremor. DSS corresponds to the time difference (ESS-SSS) and DSC is the duration of the seismic crisis corresponding to the time difference (E-SSC).

The four phases of the seismic crisis allow us to define two main time intervals (Fig. 3, Appendixes A and B):

- (1) The duration of the seismic crisis DSC is the time interval between the eruption onset, E, and the starting time of the seismic crisis itself, SSC;
- (2) The duration of the seismic swarm DSS is the time window corresponding to the largest concentration of seismic events (time interval between the seismic swarm onset SSS and its end ESS).

At Piton de la Fournaise, the duration of pre-eruptive crises was known to be short, often lower than 2 h, as compared to other volcanoes (e.g. Aki and Ferrazini, 2000). The duration of the seismic crisis DSC is plotted with respect to the elevation of the highest point of all fissures (Fig. 4a) and with respect to the distance between the highest point and the Dolomieu crater center (Fig. 4b). The figures confirm that, in most eruptions, the longer the DSC, the higher the distance from the summit is, and thus the lower the elevation is, as already observed by Aki and Ferrazini (2000) and Peltier et al. (2005). At low distances we observe a better general trend (except possibly for the post-2007 events), but when the distances to Dolomieu crater reach values of approximately 2500 m, the DSC values become greater than 4 h and may attain very large values. In Fig. 4, four eruptions with a very long DSC do not follow the general trend and correspond to the following events: June 10th 1987, March 9th 1998, January 8th 2004 and December 14th 2008. The long DSC is indicated by arrows. The high DSC value on June 10th 1987 is related to the occurrence of a short seismic crisis that starts on June 9th

and that we associated to the June 10th eruption. On March 9th 1998, the eruption marks the renewal of the eruptive activity after 6 years of rest, and the seismic crises started unusually deep at ~5 km b.s.l (versus about sea level for all other eruptions) revealing a longer vertical magma path for this eruption and thus a longer DSC. If we only consider the last part of the seismic crisis, when the seismic events are located above sea level, the DSC is approximately 1 h (Battaglia et al., 2005). Consequently, the corresponding point in Fig. 4a would not be atypical at all and would follow the general trend. Regarding the December 14th 2008 eruption, the eruptive tremor started at a very low value, suggesting that the initial flux (and therefore the ascent velocity) was low, leading to a long duration of the vertical propagation. For the January 8th 2004 eruption we were not able to identify a possible explanation of this discrepancy. The relationship between elevations and seismic crisis durations is better evidenced when considering only the eruptions occurring from 1985 to 2003, when no large distal eruption occurred.

Correlation of MgO contents with distance/elevation from the Dolomieu clearly shows that low-MgO magmas (6–7 wt.% MgO) are typical of summit activity (Appendixes A and E). On the contrary, crystal-rich (high-MgO) lavas may occur at any distance from the summit vent. This observation is consistent with emission of very crystal-rich lavas from the summit or close to the summit cone in the pre-1986 period. We also notice that eruptions occurring near the eastern coast, very far from the summit vent, can be both crystal poor (1986) or crystal-rich (2007). Peltier et al. (2009a) suggested that magmas with increasingly MgO contents are emitted at increasing distances from the vent. But our observations for the 1985–2010 period do not enable us to extrapolate.

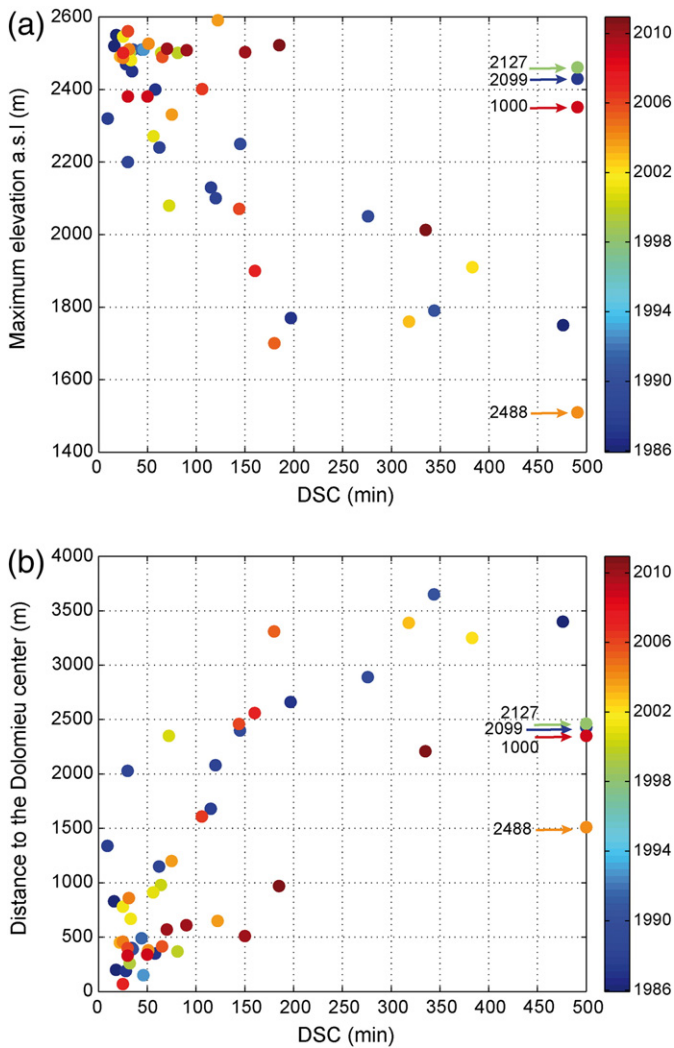


Fig. 4. Duration of the pre-eruptive seismic crisis (DSC) versus (a) maximum elevation and (b) the distance to the Dolomieu crater, during the whole December 1985–December 2010 period. The colored right hand scale indicates the dates. All eruptions are reported except for three eruptions without any evidence of seismic crises (July 13th 1986 at elevation 2470 m; March 11th 1998 at elevation 2211 m; August 30th 2006 at elevation 2501 m). Four eruptions with very large DSC values (in minutes) are reported by arrows and the DSC value is indicated near the corresponding arrow (DSC=2099 on June 10th 1987; DSC=2127 on March 9th 1998; DSC=2488 on January 8th 2004; DSC=1000 on December 14th 2008).

3.3. Seismic crises and intrusions

Different types of seismic crises that are not followed by an eruption can be distinguished in Appendix A and Fig. 2. We observe 4 distinct behaviors: seismic crises with no deformation detected (SC), seismic crises with detectable deformation (SC-D), seismic crises followed by tremor but without detectable deformation (SC-T), and seismic crises with detectable deformation followed by tremor (SC-DT). Only two SC-T and SC-DT cases have been recorded since the foundation of the OVPF observatory; they correspond to rare hour-lasting events of non-eruptive tremor, both detected after the 2007 summit collapse.

Some of these seismic crises without any eruption can be interpreted in terms of intrusions. In the literature the term “intrusion” is used to describe magma motion within a volcanic

edifice without an eruption ensuing. When deformation is associated to the seismic crisis, no doubt is possible on the nature of the seismic crisis and this case can be considered as an intrusion. In the following, the evident intrusions correspond to both SC-D and SC-DT cases, for which we identified clear deformation (either on OVPF records or on RER recordings, sometimes on both), highlighting that a dyke started but stopped before reaching the surface. The presence of a tremor following the seismic crisis for the SC-T case (September 12th 2008) proves magma degassing and magma flowage at shallow depth below the surface, and the SC-T case was included in the 11 intrusions events observed (Appendix A).

The SC-type seismic crisis is not associated with detectable deformation. The case can be interpreted either in terms of deep intrusion, too deep to generate detectable deformation on the network, or in terms of brittle failures most likely associated with hydrothermal fluid. We observed 15 SC events during the period under study.

In the 1985–2007 period, only a few seismic crises, not associated with eruptions, were recorded by the observatory networks (Appendix A). The occurrence of this kind of seismic crisis (with or without deformation) clearly increased since 2007, with 11 seismic crises in 2008, 5 in 2009 and 2 in 2010, as shown in Appendix A and Fig. 2. The high number of seismic crises (including the possible ‘intrusions’), relative to the number of eruptions, could be linked to stress changes in the volcanic edifice following the 2007 summit caldera collapse, that might have resulted from the stabilization of the collapse structure under the effect of small-volume intrusions and gravity.

4. Signals recorded by the distant RER broad-band station

4.1. Data processing

Signals of the broad-band RER station data were directly obtained from the GEOSCOPE Web site (<http://www.geoscope.fr>). We systematically downloaded the data corresponding to the vertical component and both of the horizontal ones (north–south and east–west), for long time series starting 15 days before all the volcanic events and lasting 30 days. For the 1992–2010 period, we analyzed the seismic LH or BH channels (ground velocity at 1 sample per second, sps, and 20sps respectively) and the LM channels (boom position), when available (acceleration, at 1sps). We downloaded the ground acceleration VH data, essentially for data before 1992 since it was the only continuous recorded channel (sampling rate 0.01 sps). The signals are analyzed using SAC library. First, the raw LH data (in counts) are low-pass filtered at 100 s by using Butterworth filters in order to enhance the long period transient signals. Secondly, the instrument response is removed in order to retrieve the ground velocity (in m s^{-1}). Finally, we performed a signal derivation in order to observe the acceleration signal. In what follows, we will refer to the velocity or the acceleration signal.

Fig. 5 shows the examples of three eruptions and one intrusion as recorded by the short-period station BOR (Bory) and the broad-band station RER by displaying in (A) the spectrogram obtained at BOR station, (B) the ground velocity raw data (LH signal in counts) of the north–south component at the RER station and (C) the same signal in acceleration (m s^{-2}) after a low-pass filtering at 100 s and removal of the transfer function.

4.2. Long period transient observations

The high sensitivity of the acquisition chain, the low power spectral density noise due to the isolation of the instruments

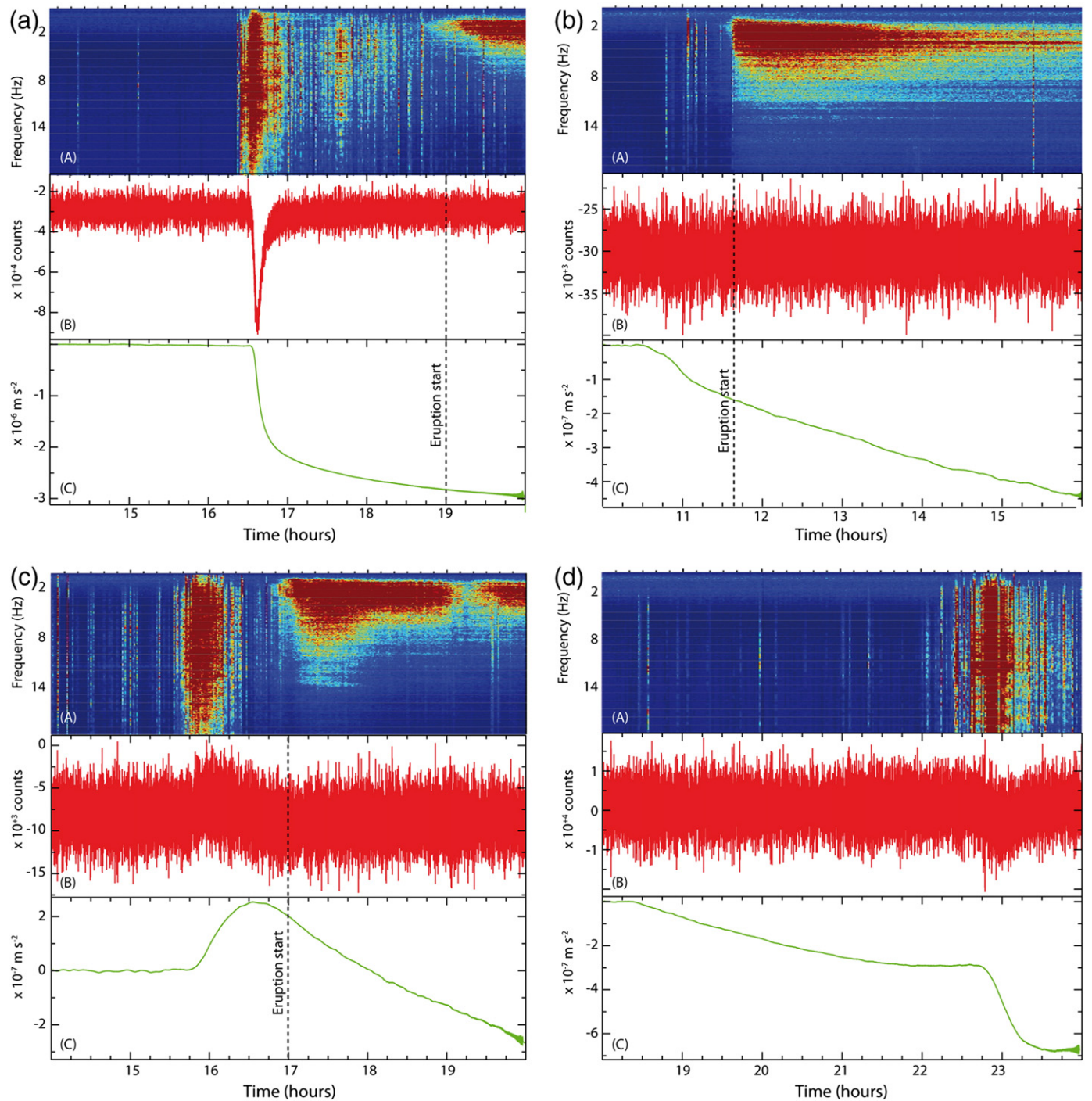


Fig. 5. Examples of seismic crises and the associated long period transient at the RER distal station. Comparison of (A) the spectrogram at the short-period BOR (Bory) station located at the summit (OVPF network), (B) the ground velocity (in counts) and (C) the acceleration trace (in m s^{-2}) at the RER station, for 3 eruptions and 1 intrusion. a) March 30th 2007 from 14 h to 20 h. b) September 21st 2008 from 10 h to 16 h. c) November 5th 2009 from 14 h to 20 h. d) Intrusion of September 23rd 2010 from 18 h to 24 h. The eruption start is indicated by a vertical dash line.

and the good environmental conditions allow us to identify subtle transient signals on the RER broad-band GEOSCOPE station linked to the preparation of Piton de la Fournaise eruptions or intrusions, despite a distance of 8.5 km between the station and the summit.

The examination of the horizontal records at RER station, highlights very long period transients (period larger than 100 s) that occur after the beginning of the seismic crisis

(SSC) and before the beginning of the eruption (examples in Fig. 5a, b, d).

These unusual long period seismic signals, observed on the horizontal components before the eruptions, are commonly interpreted as tilt signals induced by the inflation and/or deflation of the volcano (Battaglia et al., 2000; Battaglia and Bachelery, 2003). Houlié and Montagner (2007, 2009) believed that a significant part of the signal is related to ground

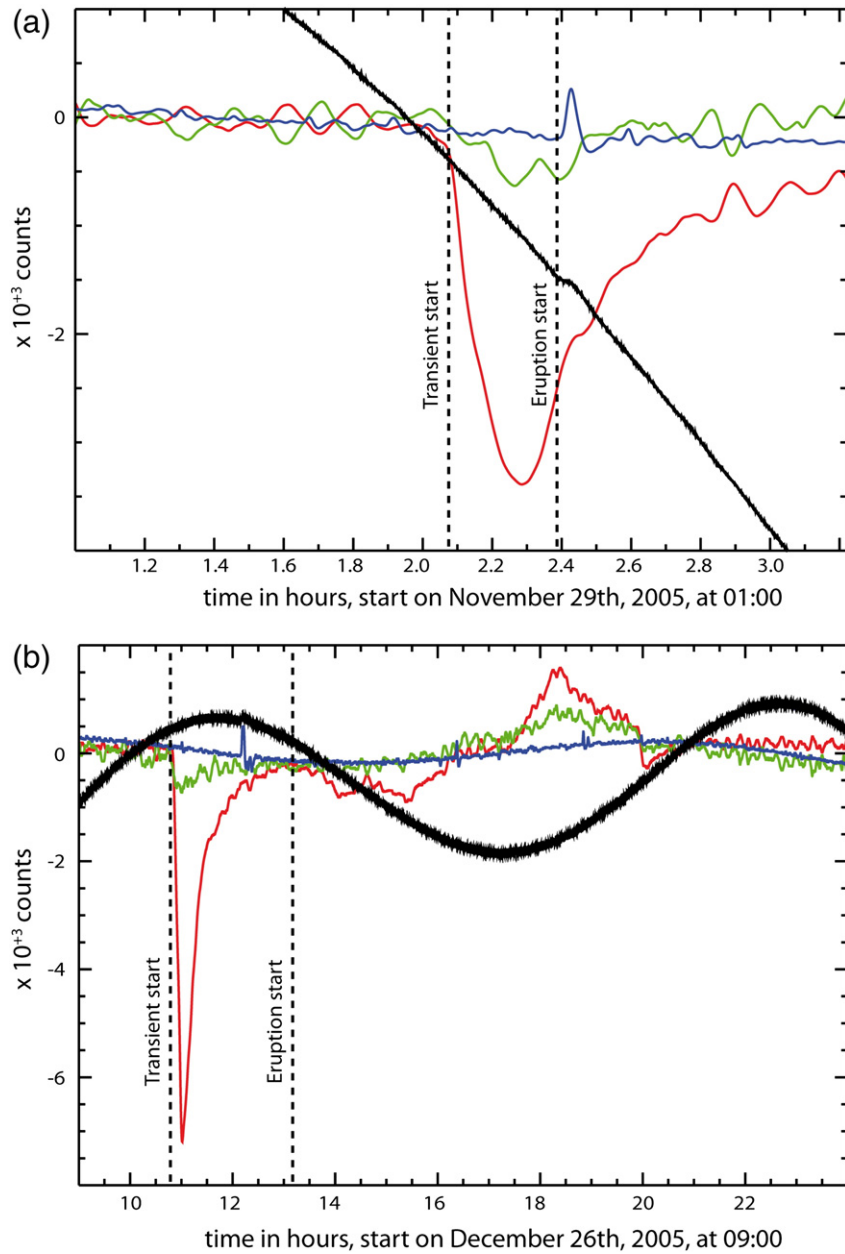


Fig. 6. Signals observed on the three seismic LH components at the RER station (Z in blue, N-S in red and E-W in green), in counts, after a low-pass filtering at 100 s. For comparison, the vertical boom position POS (LMZ channel in black) in acceleration is plotted as well with a different scale. The transient onset and the eruption onsets are indicated by dashed lines. Both eruptions show a signal on the vertical component, coeval or not with the eruption onset time. a) Eruption of November 29th 2005; b) The complex eruption of December 26th 2005 (3 fissures). (For interpretation of the references to color in this figure legend, the reader is referred to the web version of this article.)

displacement. In fact, the data collected from a single station do not allow the discriminating between tilt and displacement. The output of a horizontal component broad-band seismograph is dominated by ground displacement at short periods (<100 s), but tilt becomes a significant part of the signal at longer periods (Wielandt and Forbriger, 1999). Independently from the interpretation on tilt or displacement, the transient clearly results from pressure variation within the volcanic edifice. Such pressure variation can be related to magma injection and highlights the rupture mechanism and the dynamics of the magma transfer itself.

Moreover, the detection of the long period signal on the distal RER seismological station generally starts at the same time as

phase 2 of the seismic crisis (when existing) and extends over the third phase (Fig. 5, Appendix A). This observation may be considered as evidence of pressure source displacement (i.e. magma up-raise) during the transition from phase 2 to phase 3 of the seismic crisis.

The quasi-absence of any signal on the vertical component, and the low amplitude of the signal on the east–west component, suggest that the signal results from tilt along a north–south axis, which is radial with respect to the summit crater (Fig. 6). This hypothesis is strengthened by the tilt signals observed at the same time on the RER tiltmeter located in the same vault (Battaglia et al., 2000; Peltier et al., 2011). The transient signal is larger on the north–south component due to its orientation towards the

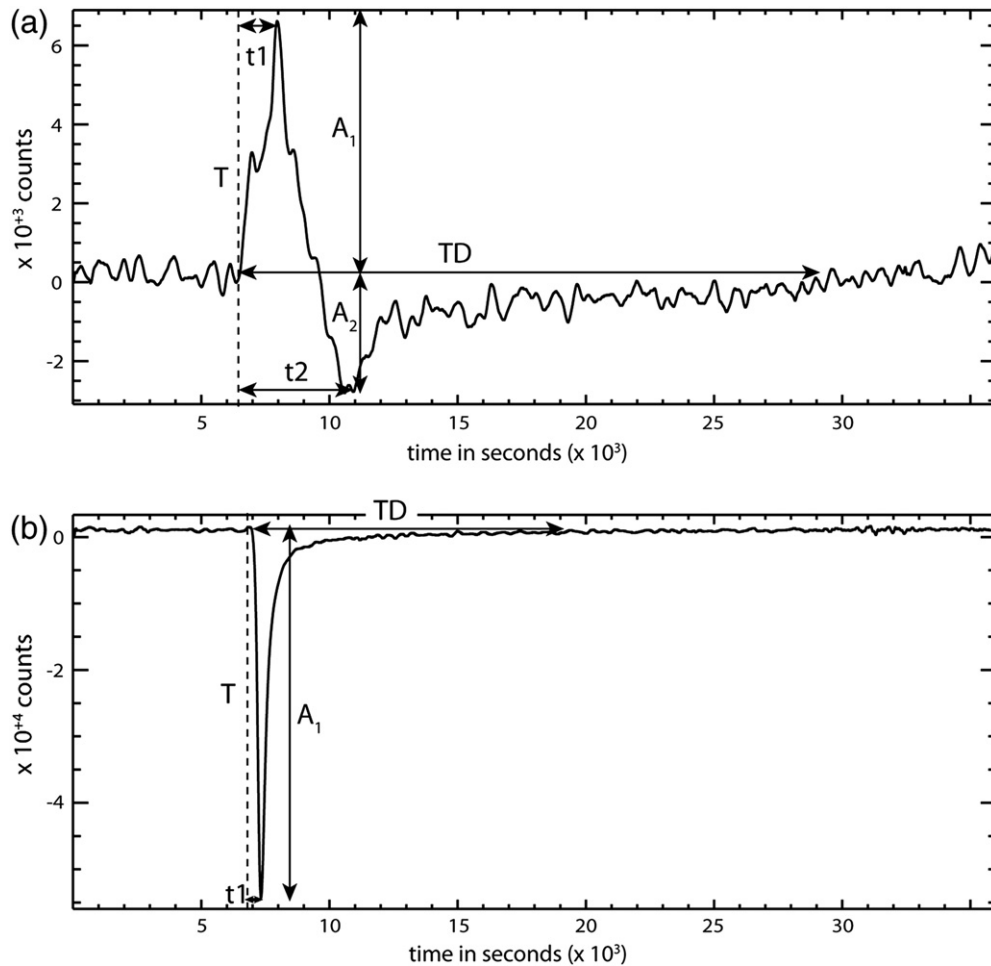


Fig. 7. Illustration of the parameters derived from the observation of transients at the RER station, for two examples of (a) Class 1 and (b) Class 2. T is the onset time of the observed transient (origin time). A_1 and t_1 are the amplitude and delay between the first extremum time and T (for both classes). A_2 and t_2 correspond to the amplitude and delay between the second extremum time and T (when existing, for Class 1 events). The TD value is the transient duration or time necessary for the signal to reach the equilibrium value.

Dolomieu crater (see Fig. 1b) and thus towards the magma pressure source (plumbing system). The transient signals on the east–west components are mentioned for few eruptions in Battaglia et al. (2000) and Houlié and Montagner (2007). We confirm its presence with lower amplitude for most of the eruptions (R_{NE} parameter). Some transient signals can be observed on the vertical component, but they are rare. The signal LMZ (boom position POS) is a very well adapted channel for such an investigation, because the response in acceleration is flat at ultra long periods. Two examples related to the eruptions of November 29th 2005 and December 26th 2005 are given on Fig. 6. The vertical signals (when existing) are not always coeval with the corresponding horizontal transient. The transients observed at RER are sometimes associated to a particular fissure index F_i specified in Appendix F and mentioned in Appendix A, but not systematically because of the difficulty of correlating one particular transient with the orientation of a given fissure.

4.3. Classes

We confirm the occurrence of two main types of transients that we named Class 1 and Class 2 as first observed by Battaglia et al. (2000), Houlié and Montagner (2007), adding information to Class 1 and Class 2 waveforms by accounting for the sense of the

first movement (Class 1+, Class 1–, Class 2+, Class 2–). The waveforms analysis helps to retrieve numerous parameters (t_1 , A_1 , t_2 , A_2 , R_{12} , TD) defined in Appendix C; some of which are illustrated in Fig. 7.

Examples of transients, illustrating the differences between Class 1 and Class 2, are given in Fig. 8a. Class 1 corresponds to a signal exhibiting two successive impulses with opposite senses. The signals of Class 2 are very simple and exhibit a unique slump. We attributed + or – to our signals, regarding the sign of the first output, “+” when the first movement is a positive impulse and “–” when it is a negative impulse.

In Appendix A, we mention 3 additional classes (0, 3 and 4):

- (1) *Class 0* corresponds to the absence of signal on the north–south recordings at RER station within a 12 hour time window before and after seismic crises. Two observed Class 0 transients are associated with low-volume eruptions; the others are associated with seismic crises without detectable deformation.
- (2) *Class 3* corresponds to pit craters or caldera collapses. There are three interesting episodes of pit crater or caldera collapses during the 1985–2010 period. There is no available data at RER corresponding to the first one in 1986 described in Hirn et al. (1991). The second one in 2002 was

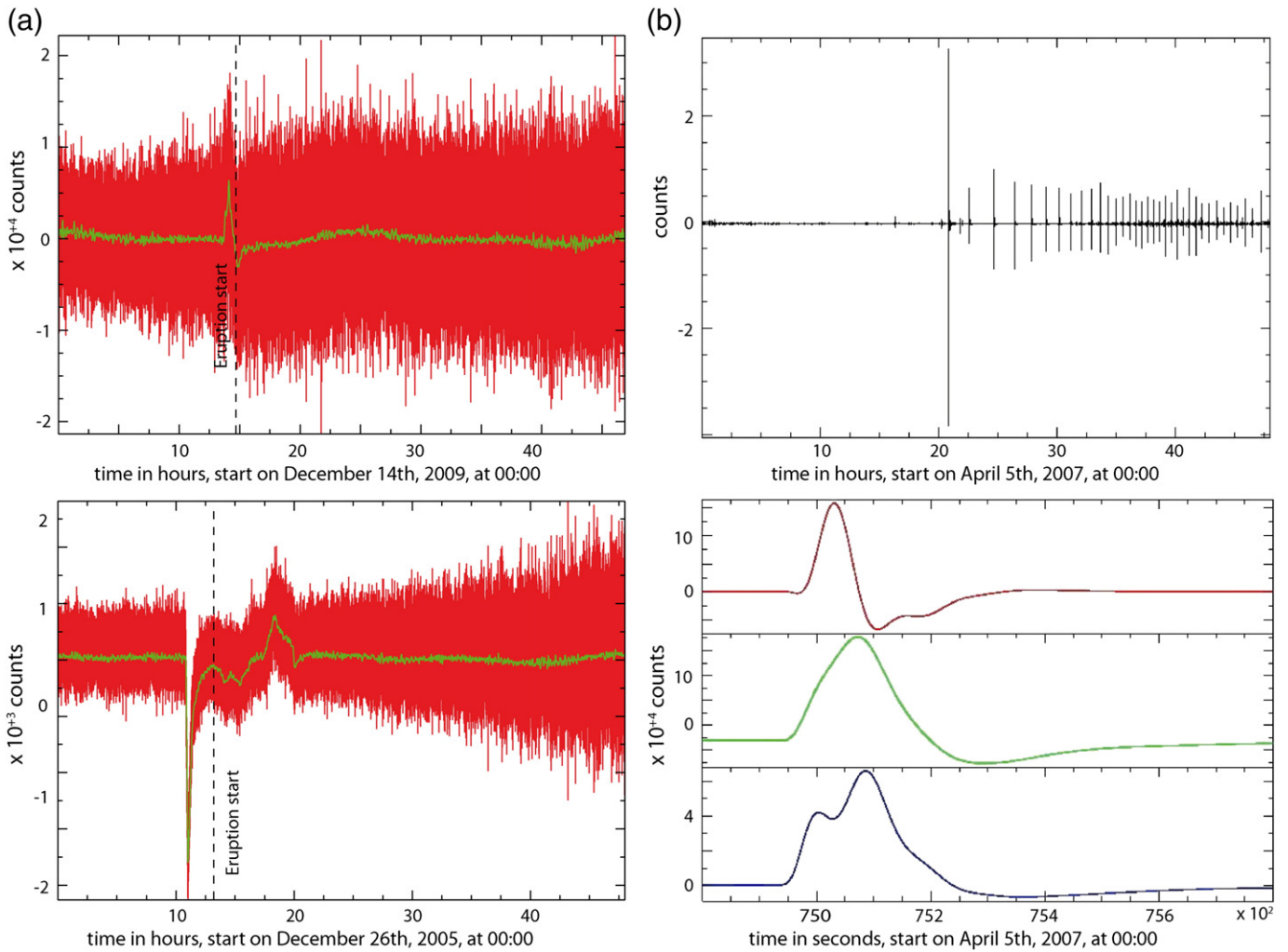


Fig. 8. Examples of transients observed at the RER station on the north–south component, on traces corresponding to the ground velocity (in counts). The red traces correspond to raw data, the green ones to the same traces after a low-pass filtering at 100 s. The black vertical dash lines indicate the eruption onset times. a) Top: Transient of Class 1+ before the December 14th 2009 eruption. Bottom: Transient of Class 2– before the December 26th 2005 eruption. b) Top: Transient of Class 3 observed during the two first days of the collapse episode of April 5th and April 6th 2007. Bottom: Velocity traces (in counts) of the first main collapse (at 20:48 GMT on April 5th 2007) for the 3 LH components, after a low-pass filtering at 100 s. (For interpretation of the references to color in this figure legend, the reader is referred to the web version of this article.)

documented by Carter et al. (2007). It provided signals of very low amplitude at the RER station, difficult to distinguish from the background noise and from the Earth tide effect; we observe a small step on the velocity signal. The third one occurred at a period of technological improvements and high-quality data, on April 5th 2007, and has been extensively studied (e.g. Michon et al., 2007; Peltier et al., 2009b; Staudacher et al., 2009). The Class 3 signals are characterized by a coeval input on all 3 components (horizontal and vertical), as seen on Fig. 8b.

- (3) Class 4 signals cannot be described by any previous class; they correspond to a small step in the velocity signal.

Most Class 1– and 2– transients were recorded during north-eastern rift zone eruptions, whose dykes propagated towards the RER station. All Class 2+ and Class 1+ transients were recorded during eruptions located inside or close to the southern rim of the Dolomieu crater (Fig. 9). The dominant transient classes are Class 2– and Class 1+ and we propose simple physical interpretation for those families (Fig. 9). Except for two eruptions, Class 2– transients are associated with lateral eruptive fissures, whereas most of

the Class 1+ transients are associated with summit or near-summit eruptions.

A current view of the magma system is described by Peltier et al. (2009a) and Massin et al. (2011). They locate the root of the dyke at the top of a shallow reservoir, situated between sea level and a few hundred meters above. We consider that the pressure sources associated with the signal recorded at the RER station are located in this region. Two pressure sources are competing during dyke intrusions, a positive one associated with the dyke itself, and a negative one linked to the magma reservoir depressurization. On one hand, the dyke effect is quite the same for all injections, since it is mainly related to physical properties of the magma and surrounding medium with a limited effect of the source conditions (Taisne and Tait, 2009, 2011). On the other hand, the degree of depressurization is more variable since it is related to relative volume changes and therefore to erupted volumes. The first signal movement characterizes either the main influence of the inflation source (sign +; e.g. the dyke) or the deflation source (sign –; e.g. the magma reservoir depressurization). Class 2– transients may correspond to dykes coming from an intermediate size reservoir for which depressurization may

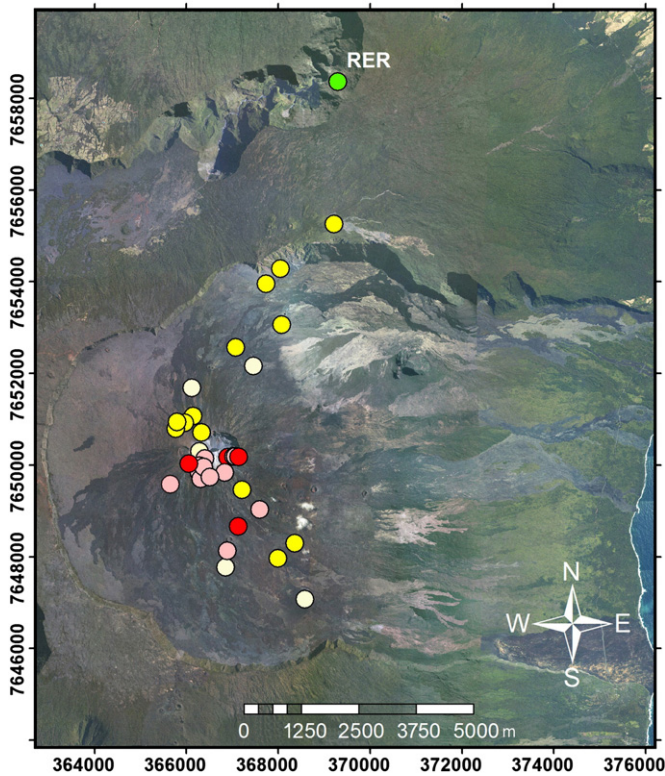


Fig. 9. Distribution of the observed RER transient class types (2+ in red, 1+ in light red, 2– in yellow, 1– in light yellow) according to the location of the first eruptive fissures. The RER station is indicated by a green dot. (For interpretation of the references to color in this figure legend, the reader is referred to the web version of this article.)

play a dominant role, hiding the effect of the dyke itself. Class 1+ transients, mainly observed for low-volume summit or near-summit eruptions, could be explained by a migrating overpressure source that is released when the dyke breaks the surface (onset of the eruptive tremor), and then the depressurization of the magma reservoir becomes visible. All sign+ transients are related to low-volume eruptions ($<10^7 \text{ m}^3$); for which the distant RER station mainly recorded the influence of the dyke and not the low depressurization of the reservoir.

On the one hand the complexity of the observed signals (family, class, polarization...) could suggest that the magma plumbing system is more complex than previously thought, with storage zones in the form of magma batches with different volumes, instead of a single reservoir, and/or with the implication of a combination of sources (deep, shallow reservoirs, dykes, sills...). On the other hand, the relative volume of the dyke, compared to the available volume of the feeding batch, may also contribute to explaining class and polarization differences. The volume and the flux of magma represent critical input parameters for modeling dyke propagation and forecasting failed eruptions (Taisne et al., 2011b). We thus correlate the volume of emitted magma with respect to the first maximum value of the north–south recording velocity (A1 – see definition on Fig. 7 after taking into account an amplification factor that depends on the transfer function at the time under study), for all velocity traces in the 1993–2010 period (Fig. 10). Most eruptions agree with a positive correlation and the large ground motions may be related to the large amount of magma involved in the dyke. Two cases (indicated by arrows and the corresponding volume values) deviate from the general trend: first, the 1998 eruption with a volume of $61.6 \times 10^6 \text{ m}^3$,

already mentioned above; second, the March 30th 2007 eruption, which preceded the exceptional April 2nd 2007 eruption, both considered as a unique eruption. Regarding the large amplitude (A value described in Appendix C) associated to March 2007 eruption, we may suppose a close link of lava flows ($240 \times 10^6 \text{ m}^3$; Bachèlery et al., 2010) between them. No clear transient was observed in April 2007, which suggests that the two events separated by only three days might belong to the same process as observed with seismicity and deformation analysis (Peltier et al., 2009b; Massin et al., 2011).

4.4. RER transient parameter

In Appendix A we compiled the RER transient characteristics for all eruptive events. Some of them are illustrated in Fig. 7.

In Fig. 11, the time difference between the transient time T and the start of the seismic crisis SSC is plotted with respect to date and with respect to the QUAL parameter (see Appendix C). Two eruptions are out of range; the first one is the June 10th 1987 eruption with a time difference reaching approximately 1960 min, but we do not have enough elements to explain that long duration. The second one is the eruption of 1998 already mentioned, with a time difference reaching more than 2060 min. In 1998, the propagation of a deep seismicity from $\sim 5 \text{ km b.s.l.}$ to sea level was observed underlining a deep magma refilling of the upper structure of the volcano edifice after 6 years of rest, too deep to be accompanied by significant ground deformation and RER transient. Only the late phase of magma propagation (from sea level to the surface) generated ground deformation and RER transient, 1 h before the start of the eruption (Battaglia and Bachèlery, 2003; Battaglia et al., 2005).

The transient onset T, likely associated with the start of magma propagation is sometimes clearly postponed regarding the start of the seismic crisis SSC. That interesting pattern becomes even more marked after the caldera formation in April 2007, with delay times that may attain more than 1 h, suggesting a change in the initial conditions of the volcano and the eruption

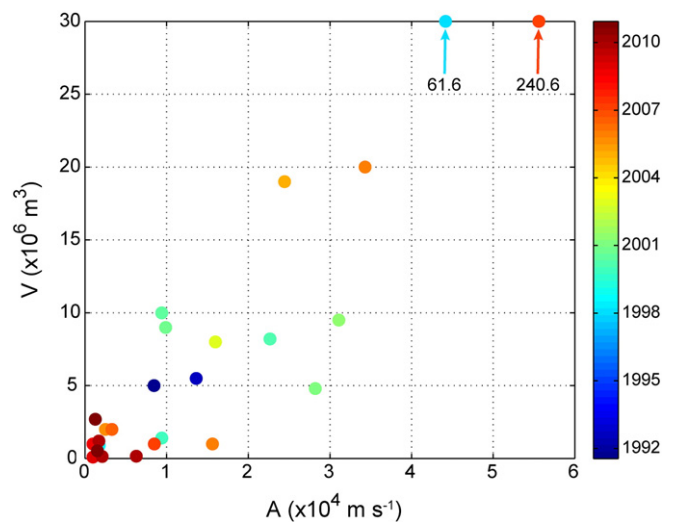


Fig. 10. Volume of lava V as a function of the A parameter. A is a value proportional to the amplitude of the first maximum of the north–south recording in velocity, after accounting for the transfer function. The right hand color bar indicates the dates. Two odd cases are indicated by arrows and their corresponding volume values (see text for details). (For interpretation of the references to color in this figure legend, the reader is referred to the web version of this article.)

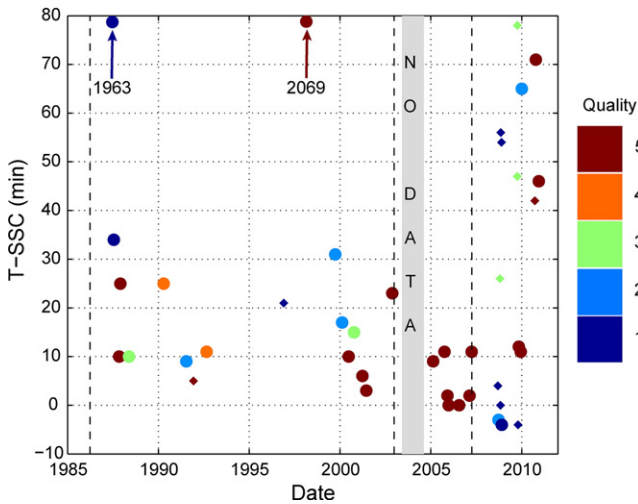


Fig. 11. Duration of the delay between the transient onset time T and the start of the seismic crisis SSC , versus time. The RER station was not operational between February 2003 and September 2004 (shadowed box). The pit crater collapses of March 29th 1986, December 23rd 2002 and the caldera collapse event of April 5–6th 2007 are indicated by vertical dash lines. Eruptions and intrusions are indicated by circles and diamonds, respectively. The right hand color bar refers to the quality of the RER transient signal (0: very noisy signal, 5: clear signal). Two extreme cases are indicated by arrows and their corresponding T - SSC value (see text for details). (For interpretation of the references to color in this figure legend, the reader is referred to the web version of this article.)

triggering. Such change can be related to distinct initial conditions, either to major stress perturbation inside the edifice induced by this extreme event (Peltier et al., 2010) or to a decrease in the volumes of magma involved in the generation of overpressure or to a major modification of the storage system after the large-volume 2007 eruption.

In most cases, the transient onset time T is very close to the start of the seismic swarm SSC ; it can be interpreted as the fracturing phase of the magma chamber's roof or of a physical barrier for magma coming from deeper regions, and the beginning of magma ascent inside the sub-aerial edifice.

The general trend of decrease in T - SSC in the 1985–2007 period could reveal a progressive weakening of the physical barrier to be overcome till the final caldera collapse event. The increase of the T - SSC interval after 2007 could indicate that at least part of the volume involved in the volcano unrest is now coming from storage regions located below sea level. For example, this zone could correspond to the low-velocity seismic zone identified at about -2 km b.s.l. by Prôno et al. (2009).

5. Discussion

5.1. "Intrusions" versus eruptions: an early warning system?

The need for volcanic hazard assessment requires significant improvements in our capability of performing precise and reliable eruption forecasts. This goal is often attained by cross-correlating various observation parameters and methods. It is of paramount importance for scientists working in an observatory and detecting the beginning of a seismic crisis, to be able to monitor the propagation of magma and to discriminate between scenarios leading to intrusions or to eruptions. One of the critical parameters determining the evolution of magma ascent towards eruption or intrusion is the volume of injected magma (Taisne et al., 2011b). On the basis of theoretical analyses and laboratory

experiments, for a given state of the volcano, magma flux has to overcome a threshold value to prevent solidification effects and sustain magma migration until it breaks the surface (Delaney and Pollard, 1982; Rubin, 1993; Bolchover and Lister, 1999; Taisne and Tait, 2009).

We analyzed the most recent eruptions for which the transfer function was perfectly well known (17 eruptions and 7 intrusions spanning the 2005–2010 period) with the aim of distinguishing whether an intrusion will stop or if it can evolve towards an eruption. The raw recordings of the north–south component of the RER station (in counts) have been derived and corrected for the transfer function in order to get acceleration signals in m s^{-2} . For each year from 2005 to 2010, and each eruptive event, we analyzed long time windows of the acceleration traces, starting 4 days before the eruptive events and lasting 8 days. In Fig. 12, all records start 1 h before the transient onset time. Transient signature is a step in acceleration that can be large or not, with slopes more or less steep according to the acceleration rate. To highlight the acceleration steps, the records have been unbent in order to flatten the signal corresponding to the first hour. The graphs of Fig. 12 show a clear differentiation between the acceleration rate of the intrusions (low rate) and the acceleration rate of the eruptions (high rate). There are two interesting exceptions:

- (1) In 2008, the different eruptions correspond to a particularly low acceleration rate as illustrated in Fig. 12b. The change in the acceleration rate during the 2008 eruptions was interpreted as due to a stress change around the magma reservoir, at least partially emptied from the caldera forming event of 2007.
- (2) The transient of September 23rd 2010 corresponded to an eruption according to our criteria, but actually it resulted in a shallow intrusion, a phenomenon previously observed by Garofalo et al. (2008). The transient was in fact a double intrusion with two consecutive different slopes, a very slow acceleration rate (intrusion) at 16:20 and another one at 22:42 (intrusion but eruption-like), as shown in Fig. 12d. The first slope is tentatively interpreted as an initial signal that reveals a small change in the stress conditions in the magma reservoir; and may be the sign of the initiation of the intrusive phenomenon. This event corresponds to the first occurrence of a long-lasting tremor without magma eruption recorded after the beginning of continuous monitoring by OVPF observatory.

We also computed the mean value of the absolute acceleration rate at different times and over different time windows (from 1 min to 10 min). For both sets of eruptive events (eruptions and intrusions), we estimated the maximum value of the acceleration rate and retrieved an average value of this maximum of $4.9583 \times 10^{-11} \text{ m s}^{-3}$ for all intrusions and an average value of $2.8642 \times 10^{-10} \text{ m s}^{-3}$ for all eruptions (Fig. 13a). With a ratio estimated to ~ 6 , the observation of the north–south component acceleration rate may allow an early identification of the two categories of events.

Fig. 13b shows the sliding average of the absolute acceleration rate obtained for the set of eruptions on one side and the set of intrusions on the other side, from 2005 to 2010. The average is calculated using 3 different sliding time windows (1, 5 and 10 min). The differences become significant after 7 min with a maximum ratio of 7. Those values change to 12 min and a ratio of 5, if we remove the exceptional event (one order of magnitude higher) associated with the March, 30th 2007 eruption. Consequently, if after 7 min from the beginning of the crisis the acceleration rate is larger than a

threshold value ($2 \times 10^{-10} \text{ m s}^{-3}$), we can assume that an eruption will most likely follow the seismic crisis.

Nevertheless, we have to stress that this approach, even if promising, can fail when dealing with either small-volume eruptions or with very shallow intrusions (e.g. the second slope I2 observed for the September 23rd 2010 intrusion in Fig. 12d). The following sections will highlight that the probability of overcoming a given threshold does not depend only on the available volume of magma or the resistance of the barriers to break, but also on other external factors.

5.2. External factors that may influence the onset of the eruption

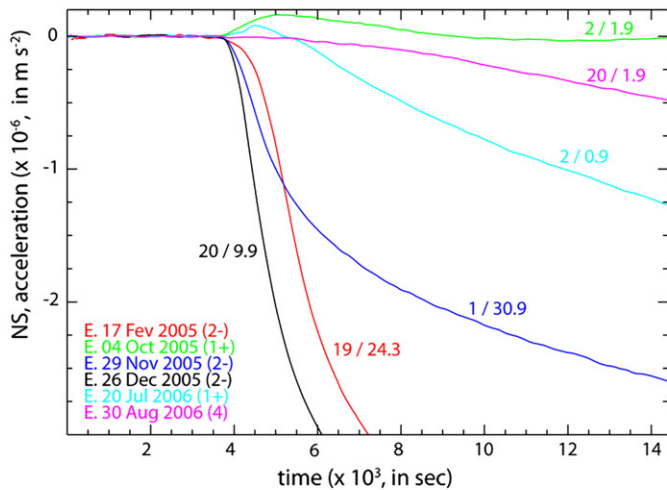
5.2.1. Influence of the rainy season

The temporal distribution of eruptions at Piton de la Fournaise is compared with the average monthly precipitation recorded by the Météo France meteorological station located at

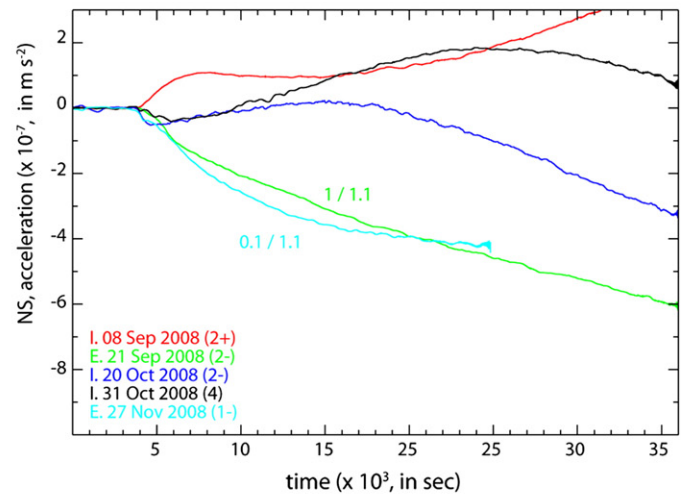
Gîte de Bellecombe (about 4 km NW of the volcano summit), for the available time series from 1999 to 2009 (Fig. 14a). The number of eruption/intrusion onsets is plotted in Fig. 14b, with respect to the month of the corresponding seismic crises, suggesting an anti-correlation between the average precipitation and the number of intrusive/eruptive events. Violette et al. (2001) previously proposed that the loading of the volcano by rainfall starts by confining the system, delaying the occurrence of a possible eruptive event. Then the discharge of the infiltrated water decreases the total load on the volcano, leading to an eruption if the magma reservoir is already close to the critical conditions to generate it. The possible link between crustal loading/unloading and volcanic/seismic activity has been long since investigated (Rampino et al., 1979; Pagli and Sigmundsson, 2008).

According to this hypothesis, possible seasonality can be proposed for the Piton de la Fournaise activity, linked to the annual

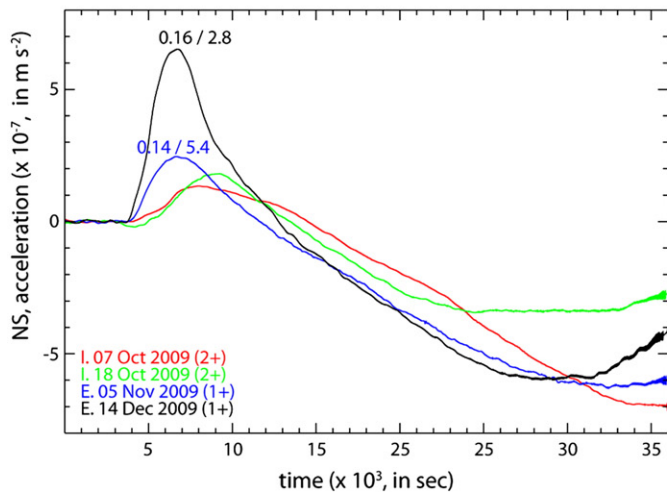
(a) Years 2005–2006, 6 eruption, duration 4 hours



(b) Year 2008, 3 intrusions and 2 eruptions, duration 10 hours



(c) Year 2009, 2 intrusions and 2 eruptions, duration 10 hours



(d) Year 2010, 1 intrusion, and 3 eruptions, duration 10 hours

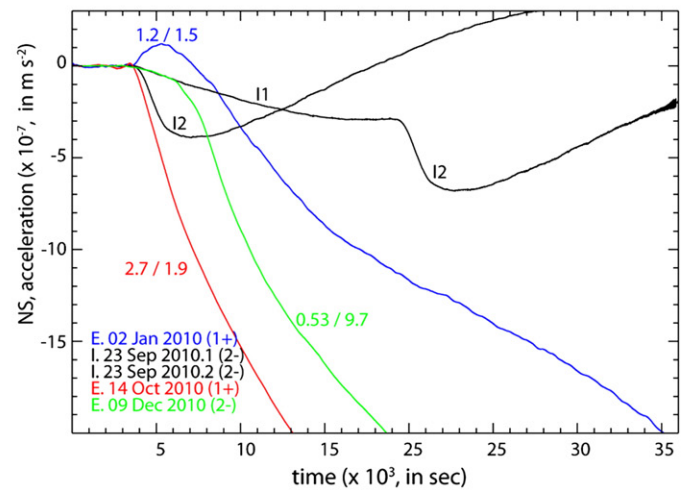


Fig. 12. The acceleration recordings (in m s^{-2}) of the NS component are plotted with time windows starting 1 h before the transient onset time and lasting 10 h (except for the years 2005–2006). The class types are indicated close to the dates (E. for eruptions and I. for intrusions). The two numbers close to the curves indicate the volume V and the mean flux FI (see Appendixes A and B). a) years 2005 and 2006, for 6 eruptions (the duration is 4 h). b) year 2008, for 3 intrusions and 2 eruptions. c) year 2009 for 2 intrusions and 2 eruptions. d) year 2010 for 1 intrusion and 3 eruptions. I1 and I2 correspond to the two distinct slopes observed for the September 23rd intrusion. The slope I2 has been plotted separately for a better comparison.

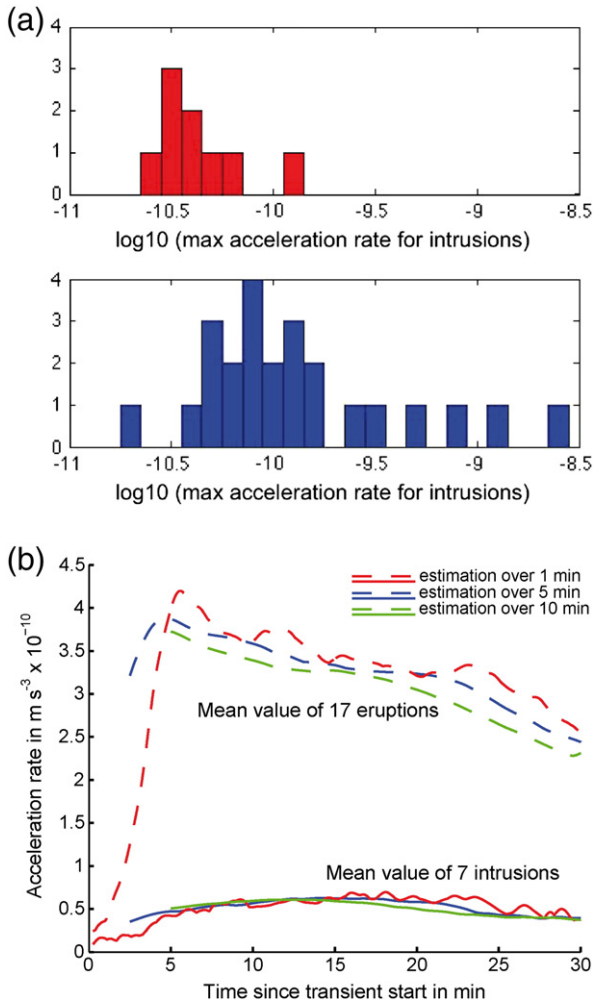


Fig. 13. Principle of the early warning system based on RER long period signal for discrimination of intrusions versus eruptions (period analysed: 2005–2010). a) Histogram illustrating the maximum value of the acceleration rate for all intrusions (in red) and eruptions (in blue). The acceleration rate (x-axis) is expressed in a logarithmic scale. The average value is $4.9583 \times 10^{-11} \text{ m s}^{-3}$ for the intrusions and $2.8642 \times 10^{-10} \text{ m s}^{-3}$ for the eruptions. b) The average values of the acceleration rate (in m s^{-3}) with respect to time are plotted from 3 different estimations sliding time windows (1, 5 and 10 min) for 17 eruptions (dash lines) and 7 ‘intrusions’ (full line). (For interpretation of the references to color in this figure legend, the reader is referred to the web version of this article.)

hydrological cycle. Moreover, the inflation/deflation evolution of the volcano edifice could also be affected by the shallow hydrothermal system (Lénat et al., 2011), which could also play a role in the evolution of the stress field.

5.2.2. Influence of earth tides

The influence of Earth tides on earthquakes has been debated for many years. Scientists have suspected a link between them for a long time, but little consensus has been reached (Omori, 1894; Schuster, 1897; Knoppoff, 1964; Hamilton, 1973; Hartzell and Heaton, 1989; Emter, 1997; Tanaka et al., 2002; Métivier et al., 2009). The role of Earth tides in triggering eruptions has also been discussed, but no clear evidence has been established until now. The interaction between Earth tide variations and other tectonic stresses is likely to be complex.

If the correlation between the tides and regional earthquakes seems difficult to establish, a possible correlation between the tides and eruptions or volcanic seismic crises, has been more easily identified, however. Tidal effects on volcanism were proposed for Pavlof in Alaska (Mac Nutt and Beavan, 1981), Mayon in the Philippines (Dzurisin, 1980), Fuego in Guatemala (Martin and Rose, 1981) and Miyakajima in Japan (Kasahara et al., 2001; Kasahara, 2002).

Two distinct classes of tides are driven by the joint gravitational attraction of the Sun and the Moon: the ocean tides and the Earth tides corresponding to slight bulges of the ocean or Earth’s surfaces (Melchior, 1983). Their theoretical calculations have been known for decades (Longman, 1959). Earth tides are smaller and less familiar than ocean tides; they go through two main cycles, a full cycle about once every 12.5 h and another cycle of a maximum height about once every 14 days. Only sensitive geophysical sensors are able to measure such small and slow ground movements. The forces that cause the eruptions are much larger in comparison to the tiny forces that produce the tides. Nevertheless, the tides might act as an additional effect for triggering an eruption, with amplitudes that may reach 10^{-7} m s^{-2} .

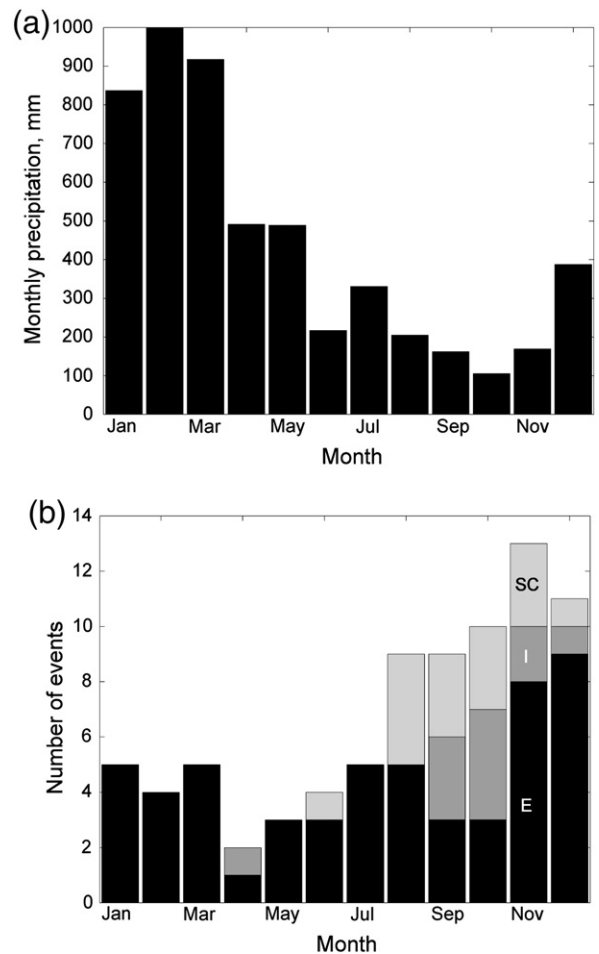


Fig. 14. a) Value of the monthly precipitation in millimetre, averaged over the 1999 to 2009 period (excluding 2005 data that was not continuously available) recorded at Gîte de Bellecombe weather station by the Meteorological French agency. b) Number of eruptive events with seismic crises (51 eruptions E in black, 11 intrusions I in dark grey and 15 seismic crises SC in light grey) with respect to the month.

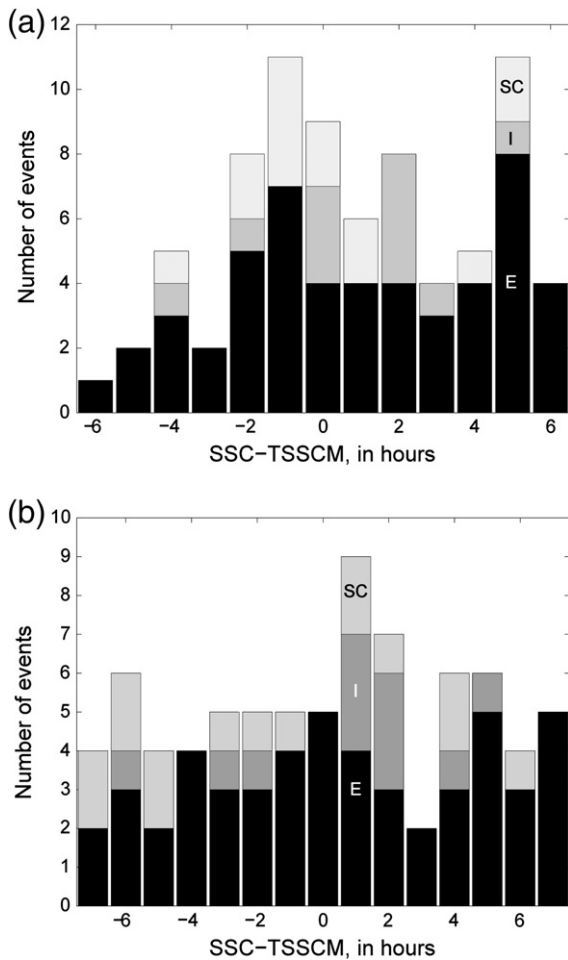


Fig. 15. Histograms illustrating the duration between the seismic crises start SSC and a) the time of maximum theoretical vertical daily tides (51 eruptions E in black; 11 intrusions I in dark grey; 14 seismic crises SC in light grey). b) The time of maximum theoretical vertical monthly tides (51 eruptions E in black; 11 intrusions I in dark grey; 15 seismic crises SC in light grey).

Using an Earth model based on the HW95 tidal potential catalog established by Hartmann and Wenzel (1995) and the free ETERNA3.30 software developed by Wenzel (1996), we computed the surface tidal theoretical vertical acceleration during the 25 years under study. For each seismic crisis event (followed by an eruption or not), we derived the dates (year:day:hh:mn) of the maximum and minimum acceleration tide closest to the start of the seismic crisis SSC and the theoretical tidal acceleration amplitude at the SSC time onset. We also determined the day closest to the SSC and corresponding to the monthly theoretical tide maximum.

We chose to compare the starting time of the seismic crisis (SSC) and the nearest calculated diurnal maximum and nearest monthly maximum of vertical tidal acceleration. We deliberately use SSC instead of the eruption onset time (E) since the tide may act on the critical state of the chamber, while the onset of eruptions is just the final product. High tidal values may favor fracturing the reservoir roof, and therefore initiate magma injection that may or may not reach the surface. The comparison between the SSC time of 76 distinct observations and the calculated diurnal maximum vertical tide close to SSC (Fig. 15a) does not display a clear correlation. The figure corresponds to only 76 events (51 E, 11 I and 14 SC) because 3 eruptions were without

any seismic crisis and the exact hour of 1 seismic crisis event was unknown.

The correlation is better between the seismic crisis onset time (SSC) and the fortnightly maximum theoretical tide, as seen on Fig. 15b. The comparison with the fortnightly maximum was possible for only 77 events (51 E, 11 I and 15 SC) due to the fact that 3 eruptions were without seismic crisis but the date of all seismic crises is known. The seismic crisis onsets are clustered around the day following the fortnightly maximum. This seems consistent with the idea that the eruption initiation is sensitive to stress change and occurs preferentially when the monthly vertical tidal acceleration is close to the maximum. A prominent concentration of eruptive onsets at the fortnightly tidal maximum was observed by some authors (Mauk and Johnston, 1973; Martin and Rose, 1981).

6. Conclusions

In this study, we established a comprehensive database of 54 eruptions, 11 intrusions, 15 seismic crises and 3 pit crater/collapse episodes of the Piton de la Fournaise volcano (La Réunion Island) spanning the December 1985–December 2010 period.

Precise information linked to timing and physical properties of all eruptive events is given, as well as the systematic search for and identification of precursor events on the horizontal records of the broad-band seismological RER station for the global GEOSCOPE network.

A statistical approach allows us to correlate different parameters and to derive characteristics and behavior of eruptions and their links with the seismic crises. Our results highlight an impact of the rainy season and fortnightly Earth tides on the seismic crisis triggering and probability of magma intrusion.

From an accurate analysis of the acceleration rate of long period seismic signal in real-time, it seems possible to establish a threshold to detect whether an observed intrusion will remain an intrusive phenomenon or whether it will turn into an eruption. The prediction of the eruption onset time seems realistic, with the exception of small-volume summit eruptions or very shallow intrusions.

The real-time calculation of the ground acceleration of the horizontal components of the RER station (after removal of the theoretical tide effects) will be integrated to the set of physical and chemical parameters usually recorded at the OVPF observatory. Our research highlights the need of integrating internal factors (ascent of magma batches; dynamics of hydrothermal systems; evolution of magma reservoirs) with external factors (seasonal evolution or rain falls and Earth tides) for a robust and reliable forecast of volcanic activity.

Acknowledgments

We wish to thank all network technical staffs for operating and maintaining the local Piton de la Fournaise network since 1980 and the GEOSCOPE Data Center (IPGP, Paris, France), the IRIS Data Center (Seattle, USA), which make the RER data available.

The software ETERNA package 'The Nanogal Software: Earth Tide Data Processing Package Eterna 3.30' is available on the GGP (Global Geodynamics Project) Web site: <http://www.eas.slu.edu/GGP/ETERNA/ETERNA34/MANUAL/ETERNA33.HTM>.

We thank the Meteorological French Agency of Sainte Clotilde (97491) for providing the monthly precipitation data.

This is an IPGP contribution, no. 3300.

Appendix A Characteristics of all eruptive events of Piton de la Fournaise volcano from 1985 to 2010. See Appendixes B, C, D and E for parameter definitions.

Characteristics of eruptions, seismic crises and collapses										
Event	Eruption timing						Site			
	Start			End		DUR	Location		Distance	Rift zone
F	Date	yyyy.ddd	hh:mm	Date	hh:mm	Days	Geographical area	Name of the cone	m	°
E-L	12/01/1985	1985.335	22:15	03/12/85	02:00	1.2	Flank S		830	
E-C	12/29/1985	1985.363	14:54	07/02/86	14:00	40.0	Dolomieu W SW		200	
E-L	03/19/1986	1986.078	02:40	19/03/86	11:20	0.4	Enclos Fouqué S SE		3400	
	03/19/1986	1986.078	20:20	23/03/86	18:00	3.9	Outside of Enclos Fouqué SE	Takamaka	8580	
	03/23/1986	1986.082	13:00	28/03/86	21:00	5.3	Outside of Enclos Fouqué SE	Pointe de la Table	13550	
Co	03/29/1986	1986.088	18:43	05/04/86	16:00	6.9	Dolomieu SE	Pit crater r = 75 m depth = 80 m		
E-C	07/13/1986	1986.194	11:10	13/07/86	18:00	0.3	Dolomieu SE	Inside pit crater	350	
	07/13/1986	1986.194	14:10	13/07/86	22:00	0.3	Dolomieu SE	Inside pit crater		
E-C	11/12/1986	1986.316	12:48	13/11/86	13:00	1.0	Dolomieu SE	Inside pit crater	350	N120
E-C	11/26/1986	1986.330	12:04	27/11/86	18:04	1.3	Dolomieu E		400	N120
E-C	12/06/1986	1986.340	03:03	06/01/87	03:00	31.0	Dolomieu W + Dolomieu E		190	
			04:03				Dolomieu W + Dolomieu E		440	
E-L	01/06/1987	1987.006	08:12	10/02/87	09:00	35.0	Flank NE		2660	
SC	06/02/1987									
E-C	06/10/1987	1987.161	11:10	28/06/87	23:00	18.5	Dolomieu E		400	
E-L	07/19/1987	1987.200	03:45	20/07/87	05:00	1.3	flank N + flank S		1680	
E-L	11/06/1987	1987.310	17:06	08/11/87	18:00	2.0	Flank N		1340	N25-30 N
	11/06/1987		17:06							
	11/06/1987		17:46							
	11/06/1987		20:39							
E-L	11/30/1987	1987.334	04:03	01/01/88	03:00	32.0	Flank S	Piton Parfait	1150	
E-L	02/07/1988	1988.038	18:30	02/04/88	18:00	55.0	Flank S		2080	N35-30 S
SC-D	04/20/1988						Dolomieu NE			
E-L	05/18/1988	1988.139	00:33	01/08/88	01:00	75.0	Flank N	Faujas-Drasche-Durandal	2030	N25-30 N
E-L	08/31/1988	1988.244	13:48	12/09/88	00:00	11.4	Flank S SW	Rivals	2400	N25-30 S
SC	11/12/1988									
E-L	12/14/1988	1988.349	09:06	28/12/88	21:50	14.5	Flank N		2890	N25-30 N
E-CL	01/18/1990	1990.018	07:12	19/01/90	02:30	0.8	Dolomieu WE + flank SE	Maillard	390	?
E-L	04/18/1990	1990.108	08:50	08/05/90	19:00	20.4	Flank S SE		3650	?
E-C	07/18/1991	1991.199	23:40	20/07/91	16:00	1.7	Dolomieu E		490	
SC-D	12/07/1991									
E-CL	08/27/1992	1992.240	07:40	23/09/92	12:00	27.2	Dolomieu W + flank SE	Zoé	150	N120
SC-D	11/26/1996									
SC	08/23/1997									
E-L	03/09/1998	1998.068	11:05	21/09/98	11:59	196.0	Flank N	Kapor	1820	N25-30 N
	08/08/1998	1998.220	22:00	15/09/98	11:59	37.6	Outside of Enclos Fouqué N		5630	N25-30 N
			22:00				Outside of Enclos Fouqué N			
			22:00				Outside of Enclos Fouqué N			
E-L	08/14/1998	1998.226	11:59	15/09/98	11:59	32.0	Outside of Enclos Fouqué N			
E-L	03/11/1998	1998.070	22:45	01/04/98	23:00	21.0	Flank W SW	Hudson	2220	N25-30 N
E-CL	07/19/1999	1999.200	14:50	31/07/99	11:59	11.9	Dolomieu E + flank E		260	N120
			14:50							
			14:56							
E-CL	07/24/1999			31/07/99	11:59		Flank E			
	09/28/1999	1999.271	07:58	23/10/99	04:45	24.9	Dolomieu W + Enclos Fouqué S	Dupavillon	370	N25-30 S
			07:58							
			08:10							
E-L	10/11/1999	1999.284		23/10/99	04:45		Enclos Fouqué S			
E-L	02/13/2000	2000.044	20:18	04/03/00	18:00	19.9	Flank N	Piton Célimène, Legros	980	N25-30 N
E-L	06/23/2000	2000.175	14:00	30/07/00	15:00	37.0	Flank E SE	Piton Parvédi	2350	N25-30 N
SC	10/06/2000									
E-L	10/12/2000	2000.286	01:05	13/11/00	17:45	32.7	Flank E SE	Piton Morgabim	910	N120
E-L	03/27/2001	2001.086	09:20	04/04/01	00:20	7.6	Flank S SE	Piton Tourkal	780	N120
E-L	06/11/2001	2001.162	09:50	07/07/01	11:00	26.0	Flank SE	Piton Madoré	670	N120
E-L	01/05/2002	2002.005	19:00	16/01/02	12:05	10.7	Flank NE + Plaine des Osmondes		3250	
	01/05/2002		19:00	16/01/02	12:05					
	01/13/2002		11:59	16/01/02	12:05	3.0				
E-L	11/16/2002	2002.320	00:56	05/12/02	12:00	19.5	Flank E	Piton Guanyin	3390	
Co	12/23/2002	2002.357	06:02				Dolomieu W SW	Pit crater r = 100 m depth = 20 m		
E-C	05/30/2003	2003.150	08:00	07/07/03	15:00	38.3	Dolomieu W SW	Piton Kaf	450	
	05/30/2003	2003.150	08:00	30/05/03	16:00	0.3	Dolomieu W SW	Piton Kaf		
	06/04/2003	2003.155	07:20	06/06/03	17:20	2.4	Dolomieu W SW	Piton Kaf		
	06/12/2003	2003.163	23:08	15/06/03	02:00	2.1	Dolomieu W SW	Piton Kaf		
	06/21/2003	2003.172	19:30	07/07/03	15:00	15.8	Dolomieu W SW	Piton Kaf		
E-CL	08/22/2003	2003.234	16:50	27/08/03	18:50	5.1	Bory + flank N	Piton Payanké	650	N25-30 N
			17:20							
			19:35							
E-L	09/30/2003	2003.273	19:40	01/10/03	07:00	0.5	Flank W SW		1200	N25-30 S
SC-D	11/06/2003						Flank S SE			
E-C	12/07/2003	2003.341	11:20	25/12/03	17:00	18.2	Dolomieu E SE		380	
E-L	01/08/2004	2004.008	22:45	10/01/04	02:00	1.1	Plaine des Osmondes		3760	
E-L	05/02/2004	2004.123	15:35	18/05/04	12:00	15.9	Flank S		860	N25-30 S
E-CL	08/12/2004	2004.225	22:40	14/10/04	03:40	62.2	Dolomieu WE + flank E	Piton Kala	460	other
E-L	02/17/2005	2005.048	16:35	26/02/05	18:00	9.1	Plaine des Osmondes		3310	

Fissures		Elevation		Lava flow			Seismic crisis			Seismic swarm			Comment
N _f	F _i	Max	Min	Surf	Vol	Flux	SSC		DSC	SSS	ESS	DSS	
		m	m	km ²	10 ⁶ m ³	m ³ s ⁻¹	yyyy.ddd	hh:mm	hh:mm	hh:mm	hh:mm	hh:mm	
		2520	2400	1.462	0.7	7.0	1985.335	21:59	00:16				
		2550	2550	0.326	7	2.0	1985.363	14:36	00:18				
		1750	1720	0.655	0.5	14.9	1986.077	18:46	07:56				
		1070	870	1.205	9	26.7	1986.077	18:46	23:54				
		120	30	0.159	4	8.7	1986.081	20:38	16:22				
		2440	2440										
2	1	2470	2400	0.018	0.27	11.0	nc	nc				Phreatic explosion	
	2	2470	2400	0.018	0.01	0.4	1986.194	13:10	01:00				
		2400	2400	0.018	0.27	3.1	1986.316	11:50	00:58				
		2450	2400	ns	0.24	2.2	1986.330	11:30	00:34				
2	1	2470	2450	0.432	2	0.7	1986.340	02:35	00:28				
	2	2470	2450										
		1770	1500	1.921	10	3.3	1987.006	04:55	03:17				
							1987.153	15:57	00:33	15:57	16:30	00:33	
		2430	2430	0.079	1	0.6	1987.160	00:11	34:59	00:11	01:00	00:49	
2		2130	1950	0.933	1	8.9	1987.200	01:50	01:55	01:53	02:52	00:59	
3	1–3	2320	2020	0.777	1.6	9.1	1987.310	16:57	00:09				
	1	2320		0.112									
	2	2150		0.113									
	3	2020		0.552									
2	1–2	2240	1900	1.530	10	3.6	1987.334	03:01	01:02				
		2100	2000	1.816	8	1.7	1988.038	16:30	02:00				
							1988.111	05:11	00:31				
		2200	1900	1.452	30	4.6	1988.139	00:03	00:30				
		2250	2150	0.880	4	4.1	1988.244	11:23	02:25				
							1988.317		00:25				
4		2050	1900	0.936	4		1988.349	04:30	04:36	04:30	08:41	04:11	
		2510	2250	0.397	0.97	14.0	1990.018	06:37	00:35				
		1790	1760	1.428	8	4.5	1990.108	03:06	05:44	03:23	04:00	00:37	
		2510	2300	0.820	5	34.4	1991.199	22:56	00:44				
							1991.341	04:50					
							1991.341	04:50					
		2510	1920	0.741	5.5	2.3	1992.240	06:54	00:46				
							1996.331	17:26	01:44				
							1997.235	06:39	00:15				
9		2461	2071	7.879	60	3.5	1998.066	23:38	35:27				
3	1–3	1680	1590	0.531	0.9	0.3	nc						
	1	1680	1680	0.500									
	2	1620	1620	0.007									
	3	1590	1590	0.024			nc						
1		2211	2191	0.443	0.75	0.4	nc						
4	1–4	2501	2000	0.879	1.3	1.3	1999.200	14:18	00:32				
	1–2	2501	2501		0.3								
	3	2461	2400		0.3								
	4	2080	2000		0.7								
5	1–5	2501	1861	0.750	1.4	0.7	1999.271	06:37	01:21				
	1	2501	2501		0.5								
	2–4	2521	1881		0.6								
	5	1871	1861		0.3								
5		2501	2231	1.788	8.2	4.8	2000.044	19:14	01:04	19:14	19:21	00:07	
6		2080	1820	2.181	10	3.1	2000.175	12:48	01:12	13:00	13:20	00:20	
							2000.280	12:35	00:21				
3		2271	1980	4.074	9	3.2	2000.286	00:09	00:56				
4		2546	1950	2.513	4.8	7.3	2001.086	08:55	00:25	09:02	09:18	00:16	
8		2481	1810	3.642	9.5	4.2	2001.162	09:17	00:33	09:25	09:36	00:11	
2	1–2	1910	1070	2.761	13	14.0	2002.005	12:37	06:23	12:37	13:25	00:48	
	1	1910	1830										
	2	1070	1070				nc	nc					
4		1760	1620	3.625	8	4.8	2002.319	19:38	05:18	19:38	20:00	00:22	
		2481					2002.336		504:00				
4	1–4	2491	2491	0.278	2.16	0.7	2003.150	07:38	00:22	07:57	07:58	00:01	
	1	2491	2491		0.16	5.6							
	2	2491	2491		0.72	3.4	nc	nc				gaz pistons	
	3	2491	2491		0.59	3.2	nc	nc				gaz pistons	
	4	2491	2491		0.69	0.5	nc	nc				gaz pistons	
7	1	2591	2209	1.687	6.2	14.1	2003.234	14:48	02:02	14:48	15:10	00:22	
1	1	2331	2196	0.508	1	24.5	2003.273	18:25	01:15	18:26	18:28	00:02	
							2003.310	02:02	04:18	02:02	02:40	00:38	
2	1–2	2526	2476	0.266	1.2	0.8	2003.341	10:29	00:51				
1	1	1510	1390	0.590	1.9	19.4	2004.007	05:17	41:28	05:17	05:18	00:01	
3	1–3	2511	2011	3.287	16.9	12.3	2004.123	15:04	00:31	15:10	15:35	00:25	
5	1–5	2487	1820	4.772	20	3.7	2004.225	22:15	00:25	22:15	22:20	00:05	
3	1–3	1700	600	4.193	19	24.3	2005.048	13:35	03:00	13:55	14:10	00:15	

VTT close to SSC						Dyke azimuth				MgO concentration	
TSSCM		TSSCm		TSSCA	TMM					Min	Max
Max		mn		Ampl	Max	Az ₁	Az ₂	DVI	DLI	Min	Max
yyyy.ddd	hh:mm	yyyy.ddd	hh:mm	~m s ⁻²	day	°	°	mn	mn	%	%
1985.335	17:25	1985.335	22:39		332					7.3	7.3
1985.363	16:25	1985.363	09:29		362					7.3	7.5
1986.077	17:33	1986.078	03:19		085	145				7.6	7.6
1986.077	17:33	1986.078	03:19		085	140				8.2	8.3
1986.082	00:22	1986.081	18:47		085	110				8.3	9.5
					085						
nc		nc			188						
1986.194	18:43	1986.194	12:58	-613	188						
1986.316	12:10	1986.316	05:58	762	319						
1986.330	10:30	1986.330	16:25	333	335						
1986.340	05:01	1986.340	00:00	302	335						
1987.006	07:23	1987.006	01:29	-36	000	57					
1987.153	17:06	1987.153	12:18	380	162						
1987.160	00:45	1987.159	18:02	889	162						
1987.199	22:20	1987.200	03:03	40	206						
1987.310	15:02	1987.310	20:35	693	310	14					
						14					
						14					
						14					
						15				6.6	6.6
1987.333	22:21	1987.334	05:03	-613	338					6.6	8.3
1988.038	16:52	1988.038	10:29	824	034					6.6	8.3
1988.111	05:16	1988.110	22:15	735	107						
1988.139	04:20	1988.138	21:21	-622	137	26				7.4	7.5
1988.244	17:27	1988.244	10:54	-1189	240					6.5	6.5
?	?	?	?		315						
1988.349	05:17	1988.348	23:55	511	345	45				8.6	8.6
1990.018	07:16	1990.018	01:12	165	025	169				6.3	6.3
1990.108	10:04	1990.108	02:17	-694	101	146				6.1	6.9
1991.199	20:40	1991.200	01:33	110	193					6.6	6.6
1991.341	01:58	1991.341	08:45	140	340						
1991.341	01:58	1991.341	08:45	140	340						
1992.240	01:52	1992.240	07:44	-956	240	124				6.5	6.7
1996.331	15:29	1996.331	21:04	673	330						
1997.235	05:29	1997.235	12:08	719	231						
1998.066	23:04	1998.067	05:53	584	071	13				5.9	7.5
nc		nc			220					7.2	7.3
nc		nc									
nc		nc									
nc		nc									
nc		nc			071					8.4	9
1999.200	19:24	1999.200	13:34	-461	194	130		28	7	6.5	6.6
1999.271	03:37	1999.271	10:03	-30	268	198	126	41	27	6.6	6.6
										6.5	6.5
nc		nc								6.5	6.6
2000.044	20:37	2000.044	14:48	576	051	-6		22	39	6.4	6.9
2000.175	06:55	2000.175	13:06	-208	169	118		23	43	6.6	7.7
2000.280	08:59	2000.280	15:58	-185	287						
2000.286	01:26	2000.285	19:19	872	287	128		15	34	6.6	8.4
2001.086	03:39	2001.086	09:35	-843	084	114		7	13	6.7	7
2001.162	06:15	2001.162	11:53	271	157	133		10	20	6.7	21.1
2002.005	06:54	2002.005	13:08	-725	-001	15	74	32	346	10.4	18.5
										13.8	28.3
2002.319	23:56	2002.319	17:52	-413	323	103				6.8	16.1
					354						
2003.150	02:16	2003.150	07:48	-346	150					7	7
2003.150	02:16	2003.150	07:48		150						
nc		nc			150					7.1	7.1
nc		nc			165					7	7
nc		nc			165					6.9	6.9
2003.234	09:56	2003.234	17:20	-497	239	17		20	125	6.7	16.7
		0:00			239						
		0:00			239						
2003.273	18:00	2003.273	23:10	618	269	203		13	42	6.7	7.1
2003.310	00:27	2003.310	06:50	666	312	144					
2003.341	14:08	2003.341	07:24	-327	342	37		56		6.5	6.5
2004.007	01:23	2004.007	08:14	-450	008	24		54	2394	8	10.6
2004.123	12:42	2004.123	19:00	317	125	191		13	6	6.8	7.5
2004.226	01:39	2004.225	18:46	-101	229	71		14	8	7	8.9
2005.048	12:15	2005.048	17:03	428	055	30		28	142	9.7	23.2

Appendix A (continued)

Characteristics of eruptions, seismic crises and collapses										
Event	Eruption timing						Site			
	Start			End			Location		Distance	Rift zone
F	Date	yyyy.ddd	hh:mm	Date	hh:mm	Days	Geographical area	Name of the cone	m	°
	02/25/2005	2005.056	16:35	26/02/05	18:00		Plaine des Osmondes			
E-C	10/04/2005	2005.277	10:35	26/02/05	18:00	12.5	Plaine des Osmondes	Trou de Sable		
E-CL	11/29/2005	2005.333	02:30	29/11/05		0.4	Dolomieu W SW	Piton Kafrine	415	
E-L	12/26/2005	2005.360	13:10	18/01/06	20:00	23.3	Dolomieu N + flank N		400	N25-30 N
			13:10	18/01/06	20:00		Enclos Fouqué N + Plaine des Osmondes		2460	
			13:10	18/01/06	20:00		Enclos Fouqué N			
			16:30				Plaine des Osmondes			
			18:30				Plaine des Osmondes			
E-L	07/20/2006	2006.201	00:06	14/08/06	15:00	25.6	flank S SW	Piton La Paix	1610	N25-30 S
E-CL	08/30/2006	2006.242	07:42	31/12/06	21:00	123.6	Dolomieu E SE	Piton Wouandzani, Piton Pongal, Piton Moinama, Piton Moinache	370	
	12/09/2006	2006.343		09/12/06			Flank E			
E-CL	02/18/2007	2007.049	12:35	19/02/07	21:00	1.4	Dolomieu WE + flank E		70	
							Flank S			
E-L	03/30/2007	2007.089	19:00	31/03/07	03:00	0.3	Flank S		2560	N120
	04/02/2007	2007.092	06:00	01/05/07	20:00	29.6	Enclos Fouqué S SE	Piton Tremblet	7420	
Co	04/05/2007	2007.095	20:48				Dolomieu	whole Dolomieu depth = 340		
SC	08/04/2008									
SC	08/15/2008									
SC	08/31/2008									
SC	09/07/2008									
SC-D	09/08/2008						Dolomieu			
SC-T	09/12/2008									
SC	09/15/2008									
E-C	09/21/2008	2008.265	11:38	02/10/08	00:20	10.5	Dolomieu SW		340	
SC-D	10/20/2008						Dolomieu			
SC-D	10/31/2008						Dolomieu			
SC	11/06/2008									
SC	11/20/2008									
E-C	11/27/2008	2008.332	07:55	28/11/08	09:00	1.0	Dolomieu SW		330	
E-C	12/14/2008	2008.349	22:55	04/02/09	19:00	51.8	Dolomieu E + Dolomieu N		310	
SC-D1	10/07/2009						Dolomieu			
SC-D2							Dolomieu			
SC	10/14/2009									
SC-DT	10/18/2009									
SC	10/30/2009									
E-L	11/05/2009	2009.309	17:00	06/11/09	00:10	0.3	Flank S SE		610	
	11/05/2009		17:00	06/11/09	00:10		Flank S SE			
	11/05/2009		17:20				Flank S SE			
E-L	12/14/2009	2009.348	14:40	15/12/09	06:30	0.7	Flank S		570	
			14:40	15/12/09	06:30		Flank S			
			14:50				Flank S			
			15:09				Flank SW			
SC	12/29/2009									
E-C	01/02/2010	2010.002	10:20	12/01/10	00:05	9.6	Dolomieu W		510	
SC	09/19/2010									
SC-D1	09/23/2010									
SC-D2	09/23/2010									
E-L	10/14/2010	2010.287	15:20	31/10/10	02:00	16.4	Flank S		2210	N25-30 S
E-L	12/09/2010	2010.343	18:15	10/12/10	09:30	0.6	Flank N		970	N25-30 N
			18:15	10/12/10	09:30		Flank N			
			18:15	10/12/10	09:30		Flank N			

Fissures		Elevation		Lava flow			Seismic crisis			Seismic swarm			Comment
N _f	F _i	Max	Min	Surf	Vol	Flux	SSC	DSC	SSS	ESS	DSS		
		m	m	km ²	10 ⁶ m ³	m ³ s ⁻¹	yyyy.ddd	hh:mm	hh:mm	hh:mm	hh:mm	hh:mm	
	1–2	1700	1200										
	3	600	600										
1		2490	2490	0.348	2	1.9	2005.277	09:30	01:05	09:40	09:50	00:10	
4		2561	2411	0.434	1	30.9	2005.333	02:00	00:30				
3	1–3	2071	1580	2.648	20	9.9	2005.360	10:46	02:24	10:50	11:03	00:13	
	1	2071	2030										
	2	1840	1750										
	3	1670	1580										
2	1–2	2401	2121	0.843	2	0.9	2006.200	22:20	01:46	22:25	22:30	00:05	
2	1–2	2501	1380	1.352	20	1.9	nc	nc					
	3	1500	1380										
3	1–2	2501	2501	0.364	1	8.6	2007.049	12:10	00:25				
	3	2470	2420										
1	1	1900	1900	0.111	0.6	20.8	2007.089	16:20	02:40	16:20	16:55	00:35	
1	1	700	590	3.625	240	93.9	2007.091	20:20	09:40				
		2480	2140										
							2008.217	14:20	00:40				
							2008.228	01:05	02:05	01:45	02:05	00:20	
							2008.244	10:02	01:08				
							2008.251	23:12	00:29				
							2008.252	23:50	01:10	24:00	24:15	00:15	
							2008.256	06:15	01:08				
							2008.259	19:08	01:02				
2	1–2	2381	2381	0.085	1	1.1	2008.265	10:48	00:50	11:03	11:10	00:07	
							2008.294	05:00	00:40	05:20	05:30	00:10	
							2008.305	00:07	00:13	00:08	00:15	00:07	
							2008.311	07:35	02:00				
							2008.325	20:45	14:00				
2	1–2	2381	2381	0.029	0.1	1.1	2008.332	07:25	00:30	07:25	07:30	00:05	
2	1–2	2351	2350	0.088	1.5	0.3	2008.349	06:15	16:40				
							2009.280	04:35	02:10	05:20	06:00	00:40	
							2009.280	04:35	02:10	05:20	06:00	00:40	
							2009.287	04:50	01:10				
							2009.291	16:20	01:55	16:22	16:50	00:28	
							2009.302	00:00	01:10				
4	1–4	2508	2310	0.092	0.14	5.4	2009.309	15:30	01:30	15:40	16:10	00:30	
	1–3	2508	2449										
	4	2386	2310										
3	1–3	2512	2451	0.145	0.16	2.8	2009.348	13:30	01:10	13:40	14:12	00:32	
	1	2512	2511										
	2	2514	2539										
	3	2479	2451										
1	1	2503	2493	0.126	1.2	1.5	2009.363	13:10	02:00				
							2010.002	07:50	02:30	08:20	09:02	00:42	
							2010.262	22:58	00:10				
							2010.266	22:00	03:30	22:20	23:50	01:30	
							2010.266	22:00	03:30	22:20	23:50	01:30	
1	1	2013	2001	0.677	2.7	1.9	2010.287	09:45	05:35	10:50	11:30	00:40	
2	1–2	2522	2360	0.269	0.53	9.7	2010.343	15:10	03:05	16:20	16:50	00:30	
	1	2522	2485										
	2	2479	2360				2010.343	15:10	03:05	16:20	16:50	00:30	

Appendix A (continued)

RER signal transient														
Event	U	Transient T		TD	CI	Q	R _{NE}	Z	t1	t2	A ₁	A	R ₁₂	Comments
F		Start		Dur					mn	mn	counts	m s ⁻¹		
		yyyy.ddd	hh:mm	mn										
E-C	V	2005.277	09:41	150	1+	5		0	9	58	530	2491	3	Weak on LHE
E-CL	V	2005.333	02:02	120	2-	5	6	2:23	15		3320	15604		Remarkable
E-L	V	2005.360	10:46	120	2-	5	12	12:09	13		7300	34310		3 slopes
	V	2005.360	10:46	120	2-									Slope 1
	V													Slope 2
	V	2005.360	19:52	38	2-	3	2	0	9		670	3149		Slope 3
E-L	V	2006.200	22:20	150	1+	5	5	0	10	40	700	3290	1	
E-CL	V	2006.242	06:11		4	1	-0.5	0						Small step
E-CL	V	2007.049	12:12	90	1+	5	2	0	11	33	8500	8500	3.5	
E-L	V	2007.089	16:31	90	2-	5	5.4	16:31	6		55600	55600		Remarkable
	V	2007.091	20:26		4			0						Change in acc slope
Co	V	2007.095	20:48		3	5	3	1	2		2E+05			50 collapses
SC	V				0	1		0						
SC	V				0	1		2:12						Z only
SC	V				0	1		6:57						Z only
SC	V				0									
SC-D	V	2008.252	23:54	79	2+	1	100	0	12		700			Long duration
SC-T	V				0									
SC	V				0	1		0						
E-C	V	2008.265	10:45	60	2-	2		0	13		970	970		
SC-D	V	2008.294	05:26	20	2-	3	-1.1	0	7		1360			2 slopes
SC-D	V	2008.305	00:07		4	1		0						Step
SC	V	2008.311	08:31		4-	1	-0.2	0			500			Step
SC	V	2008.325	21:39		4+	1		0	2		185			Step
E-C	V	2008.332	07:21	21	1-	1	100	0	7	13	970	970	3	Noisy
E-C	V	2008.349			0	1		0						
SC-D1	V	2009.280	05:22	25	2+	3	100	0	16		600			Slope 1
SC-D2	V	2009.280	05:53	56	2+	3	100	0	17		600			Slope 2
SC	V	2009.287												No data
SC-DT	V	2009.291	16:16	120	2+	1	100	1	43		1250			gaz
SC	V	2009.302			0	0		0						LHN awful
E-L	V	2009.309	15:42	100	1+	5	2	0	16	85	2100	2100	2	Slope 1
		2009.309	15:54					0						Slope 2
E-L	V	2009.348	13:41	120	1+	5	5	1	22	73	6280	6280	2	Slope 1
			13:51											Slope 2
			14:01											Slope 3
SC	V	2009.363			0	1		0						High seismicity
E-C	V	2010.002	08:55	240	1+	2	100	0	8	89	1700	1700	1.5	Long duration
SC	V	2010.262												Maintenance
SC-D1	V	2010.266	18:21	240	2-	2	100	0	9		600			Slope 1
SC-D2	V	2010.266	22:42	100	2-	5	8	0	18		4100			Slope 2
E-L	V	2010.287	10:56	240	1+	5	4.6	0	10	42	1250	1250	0.3	
E-L	V	2010.343	15:56	8	2-	5	100	0	8		1520	1520		Slope 1
		2010.343	16:11	168	2-	5	100	0	30		1520	1520		Slope 2

VTT close to SSC				Dyke azimuth				MgO concentration			
TSSCM		TSSCm		TSSCA	TMM						
Max		mn		Ampl	Max	Az ₁	Az ₂	DVI	DLI	Min	Max
yyyy.ddd	hh:mm	yyyy.ddd	hh:mm	~m s ⁻²	day	°	°	mn	mn	%	%
										9.7	11.3
										22.2	23.2
2005.277	14:50	2005.277	08:31	-1294	277	342		25	31	6.5	6.9
2005.333	00:01	2005.333	06:39	524	335	358		12	18	6.9	7
2005.360	11:42	2005.360	04:53	487	365	35		10	120	9.1	12.2
					365						
					365					24.8	24.8
2006.200	23:50	2006.200	16:32	476	205	202		15	71	6.9	7
nc		nc			236	77		35		6.8	6.9
2007.049	15:18	2007.049	08:57	-235	049	90		27		6.9	6.9
2007.089	13:10	2007.089	19:05	-57	092	118		11	129	7.2	7.4
2007.092	02:07	2007.091	19:57	-1214	092	125				7.4	30
					092						
2008.217	16:06	2008.217	10:15	484	214						
2008.228	01:55	2008.227	19:18	925	229						
2008.244	14:31	2008.244	08:33	812	243						
2008.251	23:12	2008.251	13:57	349	259						
2008.252	23:50	2008.253	05:16	519	259						
2008.256	00:53	2008.256	06:44	-520	259						
2008.259	14:18	2008.259	20:23	-1075	259						
2008.265	05:06	2008.265	12:57	-642	259	no		nd	nd	6.5	6.5
2008.294	04:57	2008.294	12:47	610	289						
2008.305	02:23	2008.304	20:47	518	303						
2008.311	08:11	2008.311	03:29	185	318						
2008.325	21:47	2008.325	15:01	-530	332						
2008.332	01:07	2008.332	07:50	-1480	332	no		25		6.5	6.5
2008.349	02:30	2008.349	09:28	-441	348	no		nd	nd	6.5	6.5
2009.280	03:01	2009.280	09:45	761	278						
2009.280	03:01	2009.280	09:45	761	278						
2009.286	23:37	2009.287	05:40	-779	278						
2009.291	14:30	2009.291	20:15	714	291						
2009.301	23:19	2009.302	05:42	722	307						
2009.309	16:37	2009.309	09:37	831	307	71		85		7.6	8.3
					307						
2009.348	13:48	2009.348	06:55	1021	349	118		60		6.5	7.1
					349						
					349						
2009.363	13:31	2009.363	06:34	1083	366						
2010.002	02:42	2010.002	09:27	-1403	001	5		121		6.4	6.8
2010.263	00:50	2010.262	18:25	510	266						
2010.267	02:13	2010.266	20:14	-596	266						
2010.267	02:13	2010.266	20:14	-596	266						
2010.287	05:54	2010.287	13:46	-99	281	164		37	237	6.6	7
2010.343	17:08	2010.343	10:21	467	339	-15		nd	nd	6.5	6.8
					339			nd	nd		

Appendix B. Definition of the characteristics of eruptions, seismic crises and collapses listed in Appendix A

<i>Type of the volcanic event</i>	
E-C	Eruption that remains inside the summit craters (Dolomieu or Bory)
E-CL	Eruption that starts inside the summit craters and propagates laterally towards lower elevation,
E-L	Eruption that starts anywhere else outside of the summit craters
Co	Summit collapse (caldera or pit crater)
SC	Seismic crisis with no detectable deformation
SC-D	Seismic crisis with detectable deformation
SC-T	Seismic crisis with no detectable deformation followed by tremor
SC-DT	Seismic crisis with detectable deformation followed by tremor
<i>Eruption timing</i>	
Start	Beginning of the eruption (date, yyyy.ddd) time (hh:mm)
End	End of the eruption (date) time (hh:mm)
DUR	Duration of the eruption in days
<i>Site</i>	
<i>Location</i>	
Geographical area	Location of the events
Name of the cone	New cone names
Distance to summit	Distance between the center of the Dolomieu crater and the point of maximum elevation of the first fissure (m)
Rift zone	Direction of the rift zone where the event ensues (after Bachèlery, 1999; Michon et al., 2009)
<i>Fissures</i>	
N_f	Number of fissures
F_i	Individual fissure index following the chronological order of fissure opening (when known)
<i>Elevation</i>	
Max	Maximum elevation (m)
Min	Minimum elevation (m)
<i>Lava flow</i>	
Surf	Surface of lava flows (km ²)
Vol	Volume of lava flows (10 ⁶ m ³)
Flux	Calculated mean effusive lava rate (Vol/DUR in m ³ s ⁻¹)
Seismic crisis	See Fig. 3
SSC	Starting time of the seismic crisis (date, yyyy.ddd) time (hh:mm) of the seismic crisis; nc means no crisis
DSC	Duration of the seismic crisis (minutes)
Seismic swarm	See Fig. 3
SSS	Starting time of the seismic swarm (hh:mm)
ESS	End of the seismic swarm (hh:mm)
DSS	Duration of the seismic swarm (minutes)
Comments	Example: deformation or not at the summit, evidence of gaz...

Appendix C. Definition of the parameters estimated from the analysis of the transient observed on the 3 components at the RER station and listed in Appendix A. Some of them are illustrated in Fig. 7

U	Raw data unit: a ground acceleration (counts) V ground velocity (count)
T transient onset time	Transient onset time (in yyyy.ddd and hh:mm)
TD	Transient duration
CL	Class
Q	Quality of the transient (= 0 very noisy signal, = 1 not clear, = 5 clear)
R_{NE}	Amplitude ratio of the north–south component first extremum over the east–west one (= 100 if there is no east–west signal)
Z	0 if there is no vertical signal
t_1	Delay between the first extremum time and T
t_2	Delay between the second extremum time and T
A_1	Amplitude (in counts) of the first extremum
A	The same amplitude as A_1 after normalization accounting for the transfer function
R_{12}	Amplitude ratio of the first extremum over the second one
Comments	Comments on the RER signal (availability, quality...)

Appendix D. Definition of the parameters computed for the theoretical Earth acceleration tide (vertical component) listed in Appendix A

TSSCM	Date of the Earth maximum acceleration daily vertical tide the closest to SSC (start of the seismic crisis) in yyyy.ddd, hh:mm; nc means no crisis
TSSCm	Date of the Earth minimum acceleration daily vertical tide the closest to SSC (start of the seismic crisis) in yyyy.ddd, hh:mm; nc means no crisis
TSSCA	Amplitude of the Earth theoretical vertical tide at the date (day and hour) time of SCS
TMM	Date of the year, the closest to SCS corresponding to the Earth maximal monthly theoretical tide

Appendix E. Definition of the dyke parameters listed in Appendix A. For eruptions before 2008, the parameters are derived from various studies already published. For eruptions after 2008, the parameters are being published for the first time

<i>Dyke azimuths</i>	
Az_1, Az_2	Azimuths of the dyke from modeling (OVPF data base; Fukushima, 2005; Fukushima et al., 2005; Peltier et al., 2007, 2008; Tinard, 2007) or azimuths estimated regarding the Dolomieu–fissure direction, if no modeling is available (OVPF database; Michon et al., 2009). Az_2 is mentioned when the dyke is not a straight line.
<i>Dyke injection</i>	
DVI	Duration of vertical dyke injection deduced from deformation data in minutes
DLI	Duration of lateral dyke injection deduced from deformation data in minutes (Peltier et al., 2005; 2009a)
MgO	'No' means no deformation. concentration
Min	Minimum concentration of MgO in lava (in %)
Max	Maximum concentration of MgO in lava (in %) (OVPF data; Bachèlery, 1999; Vlastélic et al., 2007; Peltier et al., 2009a)

Appendix F. Eruptions spanning the 1998–2011 period range: geographical coordinates of each individual fissure (starting and ending points, elevations) in WGS84 system

Date of eruption	Fissure number	UTM WGS84					
		Starting point			End point		
		x	y	z	x	y	z
9 March 1998	1	366145	7651070	2461	366053	7651259	2391
	2	366153	7651270	2401	366121	7651420	2351
	3	366151	7651500	2331	366150	7651560	2311
	4	366220	7651601	2301	366219	7651671	2281
	5	366239	7651671	2281	366238	7651751	2261
	6	366318	7651712	2261	366318	7651802	2241
	7	366328	7651802	2241	366327	7651892	2221
	8	366406	7651953	2201	366484	7652213	2161
	9	366900	7652567	2101	366852	7652367	2071
11 March 1998	1	364642	7649296	2211	364513	7649185	2191
8 August 1998	1	369214	7655259	1680	369214	7655259	1680
	2	369583	7655372	1620	369583	7655372	1620
14 August 1998	3	369789	7655744	1590	369789	7655744	1590
19 July 1999	1	366689	7650585	2501	366851	7650377	2501
	2	366931	7650348	2501	367073	7650229	2501
	3	367123	7650160	2461	367305	7649981	2400
	4	367969	7649488	2080	368111	7649289	2000
28 September 1999	1	366285	7649992	2501	366203	7650171	2501
	2	366317	7649822	2521	366043	7649120	2251
	3	365965	7648959	2201	365916	7648818	2171
	4	366564	7646905	1921	366948	7646549	1881
	5	367138	7646500	1871	367239	7646411	1861
13 February 2000	1	365966	7650928	2501	365844	7651157	2411
	2	365893	7651228	2401	365863	7651287	2371
	3	365912	7651348	2371	365861	7651427	2341
	4	365900	7651578	2321	365858	7651727	2291
	5	366079	7651609	2301	366058	7651759	2231
23 June 2000	1	367594	7649034	2080	367675	7648945	2030
	2	367715	7648896	2020	367837	7648717	1960
	3	367907	7648677	1950	367978	7648618	1930
	4	368018	7648589	1920	368078	7648539	1900
	5	368079	7648489	1900	368149	7648470	1880
	6	368406	7648792	1860	368657	7648725	1820
12 October 2000	1	367210	7649471	2271	367290	7649431	2231
	2	367390	7649462	2250	367591	7649284	2160
	3	367612	7649225	2150	367945	7648938	1980
27 March 2001	1	366276	7649842	2546	366669	7649535	2441
	2	366979	7649608	2411	367100	7649450	2321
	3	367701	7649355	2140	367806	7649276	2090
	4	367966	7649308	2140	368311	7649271	1950
11 June 2001	1	366308	7649702	2481	366318	7649652	2461
	2	366389	7649593	2451	366389	7649523	2426
	3	366559	7649524	2431	366571	7649375	2376
	4	366790	7649417	2381	366892	7649208	2251
	5	366962	7649288	2281	367125	7648940	2131
	6	367330	7649472	2251	367451	7649313	2180
	7	367689	7649525	2200	368231	7649320	1975
	8	368529	7649543	1900	368799	7649486	1810
5 January 2002	1	367769	7653705	1910	367673	7653324	1830
	2	370583	7654222	1070	370583	7654222	1070
16 November 2002	1	368361	7648302	1760	368361	7648302	1760
	2	369020	7649358	1760	369130	7649359	1780
	3	369609	7649484	1570	370009	7649527	1660
	4	369810	7649426	1600	369910	7649427	1620
23 December 2002	1	366385	7649943	2481			
30 May 2003	1	366315	7649962	2491	366315	7649962	2491
4 June 2003	2	366315	7649962	2491	366315	7649962	2491
12 June 2003	3	366315	7649962	2491	366315	7649962	2491
21 June 2003	4	366315	7649962	2491	366315	7649962	2491
22 August 2003	1	365951	7650027	2591	365954	7650004	2583
	2	365946	7650083	2581	365940	7650108	2581
	3	365947	7650113	2581	365945	7650163	2581
	4	365954	7650258	2581	365986	7650369	2581
	5	366056	7650399	2620	366056	7650399	2620
	6	366063	7651009	2471	366040	7651169	2411
	7	366508	7651884	2209	366534	7652119	2209
30 September 2003	1	365892	7649308	2331	365695	7648936	2196

Appendix F (continued)

Date of eruption	Fissure number	UTM WGS84					
		Starting point			End point		
		x	y	z	x	y	z
7 December 2003	1	366983	7650148	2476	366805	7649962	2476
	2	366736	7649876	2526	366598	7649645	2496
8 January 2004	1	368384	7653581	1510	368782	7654065	1390
2 May 2004	1	365932	7649788	2511	365881	7649638	2461
	2	365899	7649558	2441	365892	7649353	2351
	3	366300	7648027	2041	366246	7647882	2011
12 August 2004	1	366544	7650034	2466	366599	7650075	2466
	2	366629	7650065	2466	366694	7650071	2466
	3	366711	7650076	2466	366972	7650043	2466
	4	367012	7650069	2466	367087	7650139	2466
	5	367132	7650120	2487	368731	7650800	1820
17 February 2005	1	368075	7653068	1700	368275	7653860	1500
	2	369642	7654438	1200	369642	7654438	1200
	3	373167	7653757	600	373167	7653757	600
4 October 2005	1	366375	7649958	2490	366375	7649958	2490
29 November 2005	1	366328	7650712	2561	366175	7650990	2501
	2	366345	7651052	2481	366392	7651293	2411
	3	366144	7650070	2501	366183	7650191	2501
	4	366270	7650491	2501	366270	7650491	2501
26 December 2005	1	367070	7652569	2071	367177	7652850	2030
	2	367737	7653955	1840	367904	7654206	1750
	3	368043	7654288	1670	368829	7654685	1580
20 July 2006	1	365651	7649586	2401	365613	7649185	2251
	2	366071	7648770	2121	366008	7648649	2141
30 August 2006	1	366959	7650068	2481	366959	7650068	2481
	2	366837	7649792	2501	366837	7649792	2501
	3	370223	7650129	1380	370223	7650129	1380
18 February 2007	1	367135	7650180	2501	367193	7650185	2501
	2	366266	7650261	2501	367193	7650185	2501
	3	367172	7650189	2470	367344	7650211	2420
30 March 2007	1	367994	7647968	1900	368218	7650195	1900
2 April 2007	1	372435	7646721	700	372791	7646165	590
21 September 2008	1	366282	7650302	2381	366313	7650242	2381
	2	366283	7650182	2381	366333	7650162	2381
27 November 2008	1	366282	7650302	2381	366313	7650242	2381
	2	366283	7650182	2381	366333	7650242	2381
14 December 2008	1	366745	7650656	2350	366745	7650656	2350
	2	366948	7650478	2351	366948	7650478	2351
5 November 2009	1	366838	7649846	2508	366849	7649840	2449
	2	366861	7649865	2502	366933	7649878	2445
	3	367088	7649977	2464	367148	7650027	2453
	4	367412	7650116	2386	367624	7650102	2310
14 December 2009	1	366516	7649742	2512	366312	7649726	2511
	2	366296	7649763	2514	366132	7649838	2539
	3	366714	7649608	2479	366751	7649506	2451
2 January 2010	1	366055	7650039	2503	366079	7650110	2493
14 October 2010	1	366894	7648138	2013	367028	7647871	2001
9 December 2010	1	365770	7650799	2522	365769	7650931	2485
	2	365798	7650945	2479	365782	7651380	2360

References

- Aki, K., Ferrazzini, V., 2000. Seismic monitoring and modeling of an active volcano for prediction. *Journal of Geophysical Research* 105, 16617–16640.
- Bachèlery, P., 1999. Le Fonctionnement des volcans boucliers. HDR Thesis, Université de La Réunion.
- Bachèlery, P., Saint-Ange, F., Villeneuve, N., Savoye, B., Normand, A., Le Drezen, E., Barrère, A., Quod, J.-P., Deplus, C., 2010. Huge lava flow into the sea and caldera collapse, April 2007. Piton de la Fournaise volcano, Workshop on Collapse Calderas, La Réunion 2010, pp. 73–74. abstract.
- Battaglia, J., Bachèlery, P., 2003. Dynamic dyke propagation deduced from tilt variations preceding the March 9, 1998 eruption of the Piton de la Fournaise volcano. *Journal of Volcanology and Geothermal Research* 120, 289–310.
- Battaglia, J., Aki, K., Montagner, J.-P., 2000. Tilt Signals Derived from a GEOSCOPE VBB Station on the Piton de la Fournaise Volcano. *Geophysical Research Letters* 27, 605–608.
- Battaglia, J., Ferrazzini, V., Staudacher, Th., Aki, K., Cheminée, J.-L., 2005. Pre-eruptive migration of earthquakes at the Piton de la Fournaise volcano (Réunion Island). *Geophysical Journal International* 161, 549–558.
- Bolchover, P., Lister, J.R., 1999. The effect of solidification on fluid-driven fracture, with application to bladed dykes. *Proceedings of the Royal Society of London Series A* 455, 2389–2409.
- Brenguier, F., Shapiro, N.M., Campillo, M., Ferrazzini, V., Duputel, Z., Coutant, O., Nercessian, A., 2008. Towards forecasting volcanic eruptions using seismic noise. *Nature Geoscience* 1, 126–130.

- Carter, A., Wyk, Van, de Vries, B., Kelfoun, K., Bachèlery, P., Briole, P., 2007. Pits, rifts and slumps: the summit structure of Piton de La Fournaise. *Bulletin of Volcanology* 69, 741–756.
- Collombet, M., Grasso, J.-R., Ferrazzini, V., 2003. Seismicity rate before eruptions on Piton de la Fournaise volcano: implications for eruption dynamics. *Geophysical Research Letters* 30 (21), 2099, <http://dx.doi.org/10.1029/2003GL017494>, 2003.
- Delaney, P.T., Pollard, D.D., 1982. Solidification of basaltic magma during flow in a dike. *American Journal of Science* 282, 856–885.
- Delorme, H., Bachèlery, P., Blum, P.A., Cheminée, J.-L., Delarue, J.-F., Delmond, J.-C., Hirn, A., Lepine, J.-C., Vincent, P.-M., Zlotnicki, J., 1989. March 1986 eruptive episodes at Piton de La Fournaise volcano (Réunion Island). *Journal of Volcanology and Geothermal Research* 36, 199–208.
- Dzurisin, D., 1980. Influence of fortnightly earth tides at Kilauea Volcano, Hawaii. *Geophysical Research Letters* 7 (11), 925–928.
- Dzurisin, D., 2003. A comprehensive approach to monitoring volcano deformation as a window on the eruption cycle. *Reviews of Geophysics* 41 (1), 1001, <http://dx.doi.org/10.1029/2001RG000107>.
- Emter, D., 1997. Tidal triggering of earthquakes and volcanic events. In: Wilhelm, H., Zürn, W., Wenzel, H.-G. (Eds.), *Tidal Phenomena*, vol. 66 of *Lecture Notes in Earth Sciences*. Springer-Verlag, Berlin, pp. 293–309.
- Fukushima, Y., 2005. Transferts de magma au volcan du Piton de La Fournaise déterminés par la modélisation 3D de données d'interférométrie radar entre 1998 et 2000. Thesis, Université de Clermont Ferrand, France.
- Fukushima, Y., Cayol, V., Durand, P., 2005. Finding realistic dike models from interferometric synthetic aperture radar data, the February 2000 eruption at Piton de La Fournaise. *Journal of Geophysical Research* 110 (B03206), <http://dx.doi.org/10.1029/2004JB003268>.
- Garofalo, K., Staudacher, T., Kowalsky, P., Boissier, P., Galle, B., Ferrazzini, V., Villemant, B., Boudon, G., 2008. DOAS monitoring network at Piton de La Fournaise volcano (Réunion Island): installation and first results from the NOVAC projet (Abstracts) *Geophysical Research* 10 (EGU2008-A-10023).
- Hamilton, W.L., 1973. Tidal cycles of volcanic eruptions: fortnightly to 19 year periods. *Journal of Geophysical Research* 78 (17), 3363–3375.
- Hartmann, T., Wenzel, H.-G., 1995. The HW95 tidal potential catalogue. *Geophysical Research Letters* 22, 3553–3556.
- Hartzell, S., Heaton, T., 1989. The fortnightly tide and the tidal triggering of earthquakes. *Bulletin of the Seismological Society of America* 79 (4), 1282–1286.
- Hirn, A., Lépine, J.C., Sapin, M., Delorme, H., 1991. Episodes of pit-crater collapse documented by seismology at Piton de la Fournaise. *Journal of Volcanology and Geothermal Research* 47, 89–104.
- Houlié, N., Montagner, J.-P., 2007. Hidden Dykes detected on Ultra Long Period (ULP) seismic signals at Piton de la Fournaise volcano. *Earth and Planetary Science Letters* 261.
- Kasahara, J., 2002. Perspectives. *Geophysics: Tides, earthquakes, and volcanoes*. *Science* 297, 348–349, <http://dx.doi.org/10.1126/science.1074601> (n°5580).
- Kasahara, J., Nakao, S., Kokets, K., 2001. Tidal influence on the 2000 Miyakejima eruption and its implications for hydrothermal activity and volcanism. *Proceedings of Japan Academy Series B: Physical and Biological Sciences* 77B, 98–103.
- Knoppoff, L., 1964. Earth tides as a triggering mechanism for earthquakes. *Bulletin of the Seismological Society of America* 54, 1865–1870.
- Lénat, J.-F., Bachèlery, P., Bonneville, A., Hirn, A., 1989. The beginning of the 1985–1987 eruptive cycle at Piton de La Fournaise (La Réunion); new insights in the magmatic and volcano-tectonic systems. *Journal of Volcanology and Geothermal Research* 36, 209–232.
- Lénat, J.F., Bachèlery, P., Peltier, A., 2011. The interplay between collapse structures, hydrothermal systems and magma intrusions: the case of the central area of Piton de La Fournaise volcano. *Bulletin of Volcanology*, <http://dx.doi.org/10.1007/s00445-011-0535-3>.
- Lengliné, O., Marsan, D., Got, J.-L., Pinel, V., Ferrazzini, V., Okubo, P.G., 2008. Seismicity and deformation induced by magma accumulation at three basaltic volcanoes. *Journal of Geophysical Research* 113, B12305, <http://dx.doi.org/10.1029/2008JB005937>.
- Longman, I.M., 1959. Formulas for computing the tidal accelerations due to the moon and the sun. *Journal of Geophysical Research* 64, 2351–2355.
- Mac Nutt, S.R., Beavan, R.J., 1981. Volcanic earthquakes at Pavlof volcano correlated with the solid Earth tide. *Nature* 294, 615–618.
- Martin, D.P., Rose, W.L., 1981. Behavior Patterns of Fuego Volcano, Guatemala. *Journal of Volcanology and Geothermal Research* 10, 67–81.
- Massin, F., Ferrazzini, V., Bachèlery, P., Nercessian, A., Duputel, Z., Staudacher, T., 2011. Structures and evolution of the plumbing system of Piton de la Fournaise volcano inferred from clustering of 2007 eruptive cycle seismicity. *Journal of Volcanology and Geothermal Research* 202 (1–2), 96–106.
- Mauk, F.J., Johnston, M.J.S., 1973. On the triggering of volcanic eruptions by Earth tides. *Journal of Geophysical Research* 78, 3356–3362, <http://dx.doi.org/10.1029/JB078i017p03356>.
- Melchior, P., 1983. *The tides of the planet Earth*. Pergamon, New-York, 641p.
- Métivier, F., de Viron, O., Conrad, C.P., Renault, S., Diamant, M., Patau, G., 2009. Evidence of earthquake triggering by the solid earth tides. *Earth and Planetary Science Letters* 278, 370–375, <http://dx.doi.org/10.1016/j.epsl.2008.12.024>.
- Michon, L., Staudacher, T., Ferrazzini, V., Bachèlery, P., Marti, J., 2007. April 2007 collapse of Piton de La Fournaise: a new example of caldera formation. *Geophysical Research Letters* 34 (L21301), <http://dx.doi.org/10.1029/2007GL031248>.
- Michon, L., Cayol, V., Letourneur, L., Peltier, A., Villeneuve, N., Staudacher, T., 2009. Edifice growth, deformation and rift zone development in basaltic setting: insights from Piton de la Fournaise shield volcano (Réunion Island). *Journal of Geophysical Research* 114, 14–30.
- Omori, F., 1894. Investigation on aftershocks. *Report of Improvement Earthquake Investigational Communications* 2, 103–139.
- Pagli, C., Sigmundsson, F., 2008. Will present day glacier retreat increase volcanic activity? Stress induced by recent glacier retreat and its effect on magmatism at the Vatnajökull ice cap, Iceland. *Geophysical Research Letters* 35, L09304, <http://dx.doi.org/10.1029/2008GL035110>.
- Peltier, A., 2007. Suivi, modélisation et évolution des processus d'injections magmatiques au Piton de La Fournaise (Réunion), Ph.D. thesis, Saint Denis, Université de La Réunion, Institut de Physique du Globe de Paris, Paris, France.
- Peltier, A., Ferrazzini, V., Staudacher, T., Bachèlery, P., 2005. Imaging the dynamics of dyke propagation prior to the 2000–2003 flank eruptions at Piton de La Fournaise, Reunion Island. *Geophysical Research Letters* 32 (22), L22302, <http://dx.doi.org/10.1029/2005GL023720>.
- Peltier, A., Staudacher, T., Bachèlery, P., 2007. Constraints on magma transfers and structures involved in the 2003 activity at Piton de La Fournaise from displacement data. *Journal of Geophysical Research* 112 (B03207), <http://dx.doi.org/10.1029/2006JB004379>.
- Peltier, A., Bachèlery, P., Staudacher, T., 2009a. Magma transport and storage at Piton de La Fournaise (La Réunion) between 1972 and 2007: a review of geophysical and geochemical data. *Journal of Volcanology and Geothermal Research* 184 (1–2), 93–108.
- Peltier, A., Staudacher, T., Bachèlery, P., Cayol, V., 2009b. Formation of the April 2007 caldera collapse at Piton de La Fournaise volcano: insights from GPS data. *Journal of Volcanology and Geothermal Research* 184 (1–2), 152–163.
- Peltier, A., Staudacher, T., Bachèlery, P., 2010. New behavior of the Piton de La Fournaise volcano feeding system (La Réunion Island) deduced from GPS data: Influence of the 2007 Dolomieu crater collapse. *Journal of Volcanology and Geothermal Research* 192, 48–56.
- Peltier, A., Staudacher, T., Bachèlery, P., 2011. Early detection of large eruptions at Piton de La Fournaise volcano (La Réunion Island): contribution of a distant tiltmeter station. *Journal of Volcanology and Geothermal Research* 199, 96–104.
- Prôno, E., Battaglia, J., Monteiller, V., Go, J.-L., Ferrazzini, V., 2009. P-wave velocity structure of Piton de la Fournaise volcano deduced from seismic data recorded between 1996 and 1999. *Journal of Volcanology and Geothermal Research* 184 (1–2), 49–62.
- Rampino, M.R., Self, S., Fairbridge, R.W., 1979. Can rapid climatic change cause volcanic eruptions? *Science* 206 (4420), 826–829.
- Romanowicz, B., Karzewski, J.-F., Cara, M., Bernard, P., Borsenberger, J., Cantin, J.-M., Dole, B., Fouassier, D., Koenig, J.-C., Morand, M., Pillet, R., 1991. The GEOSCOPE Program: present status and perspectives. *Bulletin of the Seismological Society of America* 81, 243–264.
- Roult, G., Montagner, J.-P., Romanowicz, B., Cara, M., Rouland, D., Trampert, J., Pillet, R., Karzewski, J.-F., Rivera, L., Stutzmann, E., Maggi, A., Lépine, J.-C., and the GEOSCOPE team, 2010. The GEOSCOPE Program: progress and challenges during the past 30 years. *Seismological Research Letters* 81, 427–452, <http://dx.doi.org/10.1785/gssrl1.81.3.247> (n°3).
- Rubin, A.M., 1993. On the thermal viability of dikes leaving magma chambers. *Geophysical Research Letters* 20 (4), 257–260.
- Sapin, M., Hirn, A., Lépine, J.-C., Nercessian, A., 1996. Stress failure and fluid flow deduced from earthquakes accompanying eruptions at Piton de la Fournaise volcano. *Journal of Volcanology and Geothermal Research* 70, 145–167.
- Schuster, 1897. On lunar and solar periodicities of earthquakes. *Proceedings of the Royal Society of London* 61, 455–465.
- Staudacher, T., Piton de la Fournaise Research Team, 1992–2008. *Bulletin of the Global Volcanism Network*. Smithsonian Institution.
- Staudacher, T., Ferrazzini, V., Peltier, A., Kowalski, P., Boissier, P., Catherine, P., Lauret, F., Massin, F., 2009. The April 2007 eruption and the Dolomieu crater collapse, two major events at Piton de la Fournaise. *Journal of Volcanology and Geothermal Research* 184 (1–2), 126–137.
- Stieljes, L., Moutou, P., 1989. A statistical and probabilistic study of the historic activity of Piton de la Fournaise, Réunion Island, Indian Ocean. *Journal of Volcanology and Geothermal Research* 36, 67–86.
- Taisne, B., Tait, S., 2009. Eruption versus intrusion? Arrest of propagation of constant volume, buoyant, liquid-filled cracks in an elastic, brittle host. *Journal of Geophysical Research* 114 (B6), B06202, <http://dx.doi.org/10.1029/2009JB006297>.
- Taisne, B., Tait, S., 2011. The effect of solidification on a propagating dike. *Journal of Geophysical Research* 116, B01206, <http://dx.doi.org/10.1029/2009JB007058>.
- Taisne, B., Brenguier, F., Shapiro, N.M., Ferrazzini, V., 2011a. Imaging the dynamics of magma propagation using radiated seismic intensity. *Geophysical Research Letters* 38, L04304, <http://dx.doi.org/10.1029/2010GL046068>.
- Taisne, B., Tait, S., Jaupart, C., 2011b. Conditions for the arrest of a vertical propagating dyke. In: Roman DC, Moran SC, Newhall CG (eds) *Failed eruptions: Late-stage cessation of magma ascent*, *Bull. Volcanol.* 73(2):191–204, <http://dx.doi.org/10.1007/s00445-010-0440-1>.
- Tanaka, S., Ohtake, M., Sato, H., 2002. Evidence for tidal triggering of earthquakes as revealed from statistical analysis of global data. *Journal of Geophysical Research* 107, 2211–2212, <http://dx.doi.org/10.1029/2001JB001577>.
- Tanguy, J.C., Bachèlery, P., Le Goff, M., 2011. Archeomagnetism of Piton de la Fournaise: Bearing on volcanic activity at La Réunion Island and geomagnetic secular variation in Southern Indian Ocean. *Earth and Planetary Science Letters* 303, 361–368, <http://dx.doi.org/10.1016/j.epsl.2011.01.019>.
- Tinard, P., 2007. Caractérisation et modélisation des déplacements du sol associés à l'activité volcanique du Piton de la Fournaise, île de La Réunion, à partir de données interférométriques. Thesis, Université de Clermont Ferrand, 334 pp.
- Violette, S., de MG, Carbonnel, J.P., Goblet, P., Ledoux, E., Tijani, S.M., Vuille, G., 2001. Can Rainfall Trigger Volcanic Eruptions? A mechanical stress model of an active volcano : Piton de la Fournaise, 13. Réunion Island, Terra Nova, pp. 18–24.
- Vlastélic, I., Peltier, A., Staudacher, T., 2007. Short-term (1998–2006) fluctuations of Pb isotopes at Piton de la Fournaise volcano (Réunion Island): origins and

- constrains on the size and shape of the magma reservoir. *Chemical Geology* 244, 202–220.
- Wenzel, H.G., 1996. The Nanogal Software: Earth tide data processing package ETERNA 3.3. *Bulletin Information Marées Terrestres* 124, 9425–9439 Software downloadable at the Global of Geodynamics Project Web site: <http://www.eas.slu.edu/GGP>.
- Wielandt, E., Forbriger, T., 1999. Near-field seismic displacement and tilt associated with the explosive activity of Stromboli. *Annali di Geofisica* 42 (407–416), 1999.
- Wielandt, E., Streckeisen, G., 1982. The leaf-spring seismometer: design and performances. *Bulletin of the Seismological Society of America* 72 (2349–2367), 1982.